ORIGINAL PAPER

WRF sensitivity simulations of a dense advection fog event in Istanbul

Yasemin Ezber[1] · Omer L. Sen[1]

Abstract

This study investigates the predictability of the dense advection fog over Istanbul on February 19, 2014, which significantly halted international as well as local transportation. Sensitivity simulations were conducted using the Weather Research and Forecasting (WRF) model forced by the ERA-Interim reanalysis data. A hierarchical approach was adopted. The first group of sensitivity simulations involving different microphysics schemes (WSM6, Morrison, Thompson-aerosol, NNSL, NNSL-CCN, and Milbrandt) indicated that the simulation with Milbrandt reproduced slightly better results for the fog event. Further sensitivity tests involving different planetary boundary layer (PBL) schemes (ACM2, BouLac, MYJ, MYNN2.5, MYNN, and YSU) were conducted. The YSU PBL scheme provided better diurnal air and dew point temperature variations compared to the observations at Ataturk and Sabiha Gokcen airports. We further investigated the performances of RRTMG, RRTMG-fast and Dudhia shortwave radiation schemes, and RRTMG and RRTM longwave radiation schemes. Our analyses revealed that simulation of the fog was very sensitive to radiation scheme. Although all PBL schemes were able to generate fog, a configuration with the YSU PBL scheme with Dudhia shortwave and RRTM longwave schemes produced comparatively low RMSE for temperature depression, 0.31 °C (0.23 °C), during the fog hours at Sabiha Gokcen (Ataturk) Airport. The model simulated the onset time of the afternoon fog well; however it reproduced the onset and dissipation times of the morning fog earlier than the observations. It is also found that the use of high-resolution initial and boundary condition data did not provide a significant improvement in the advection fog simulation.

Keywords Advection fog · Physics parameterizations · Sensitivity simulations · WRF

1 Introduction

Fog is an important meteorological phenomenon, which occurs at or near the surface due to the suspended tiny ice crystals or water droplets in the atmosphere. It adversely affects aviation, navigation, and land transportation. Low horizontal visibility (less than 1 km) as a result of fog might cause substantial economic losses (Bergot et al. 2007; Gultepe et al. 2007; Stolaki et al. 2012). Istanbul is a significant transfer hub connecting Europe to Asia with three airports, the newly opened Istanbul, Sabiha Gokcen, and cargo-only Ataturk airports. The Bosphorus is also an important waterway connecting the Black Sea with the Mediterranean Sea, and therefore it is subject to substantial international commercial shipping traffic. Accurate forecasting of fog for Istanbul is thus essential to reduce the associated delays and economic losses in both national and international transportation.

One common fog type, advection fog, is associated with the advection of a warm moist air mass across a cold underlying surface. Advection fog is the main type that forms often where cold ocean currents are observed; for example, in the Grand Banks of Newfoundland in the coastal northeastern US, in the North Pacific, off the west coast of North America, and over the British Isles (Lewis et al. 2004; Koracin et al. 2001), and the Yellow Sea (Gao et al. 2007; Zhang et al. 2011). Because Istanbul is surrounded by two water bodies, the Black Sea in the north and the Sea of Marmara in the south, it is also subject to advection-type fogs frequently.

Thermodynamic, dynamic, radiative, aerosol, and microphysical processes are crucial in the development and extent of fogs. Many observational and numerical studies have been carried out to better understand these processes that are influenced by the surface conditions. Field experiments were conducted in Canada (Gultepe et al. 2009), Paris, France

✉ Yasemin Ezber
  ezber@itu.edu.tr

1   Eurasia Institute of Earth Sciences, Istanbul Technical University, Istanbul, Turkey

(Haeffelin et al. 2010; Dupont et al. 2012), and Nanjing, China (Liu et al. 2011). Remote sensing methods have been used to measure horizontal visibility in fog events since the 1970s (e.g., Gultepe et al. 2007). Several techniques have been used for the detection of fog or low stratus; for instance, Eyre et al. (1984) and Turner et al. (1986) applied a dual-channel technique to the nighttime observations of the polar trajectory satellite sensor, AVHRR (advanced very high–resolution radiometer). The observations of a geosynchronous satellite, METEOSAT MVIRI, have also been used to identify the fog/low stratus by Karlsson (1989); Güls and Bendix (1996), and Cermak et al. (2009). Bendix et al. (2006) developed a radial-transfer classification scheme for MODIS Aqua and Terra observations to detect the fog/low stratus. Studies have been conducted to integrate satellite data with synoptic observations, ground observations, and numerical models (e.g., Herzegh et al. 2006). Hutchison et al. (2006), Ellrod (2002), and Ellord and Gultepe (2007) have combined prediction model outputs with satellite observations and verified them using ground observations. Models are used for the prediction of visibility, surface temperature, relative humidity, and physical thickness of fogs, while satellite observations are utilized to obtain information about the horizontal range of fogs (Gultepe et al. 2007).

Mesoscale models are widely used for examining turbulence, radiation, microphysics, and land-surface processes. Zhou and Du (2010) used the WRF model with the ensemble approach for fog forecasting in eastern China. Stolaki et al. (2011) and Roman-Cascon et al. (2012) investigated the characteristics of fogs in Greece and Spain, respectively. Results of the Paris fog measurement campaign in 2011 indicated that WRF might well represent local conditions for analysis of past fog events (Menut et al. 2013). Steenveld et al. (2015) tried to predict a radiation fog event in Cabauw using HARMONIE (HIRLAM ALADIN Research on Mesoscale Operational NWP In Europe) and WRF models, and the results were evaluated against micrometeorological measurements. Their results showed that the WRF model better reproduced the fog event in the region. Although there have been some efforts to improve the numerical weather prediction (NWP) models for fog forecasting, they are still poor in this regard due to the complexity of the interactions between several processes (Bergot et al. 2007; Gultepe et al. 2009; Muller et al. 2010; Roman-Cascon et al. 2012; Price et al. 2015; Steeneveld et al. 2015). Sensitivity studies have been conducted to improve the prediction of different types of fogs. Some involved the effect of initial conditions (e.g., Remy et al. 2009; Hu et al. 2014; Bari et al. 2015), and some tried to determine proper vertical and horizontal resolutions (e.g., Tardif 2007; Tang et al. 2009). Pithani et al. (2019a) evaluated the performance of the WRF model for an advection fog using different PBL and microphysics parameterizations, and they concluded that none of the cases outperformed the others in terms of fog prediction. Another study by Pithani et al. (2019b), which investigated the performance of different local PBL and microphysics parameterizations for a dense winter fog event, concluded that the six local PBL schemes yield small differences in the onset time for the fog life cycle, however, the thermodynamic relationship is very poor for these schemes due to the substantial bias in surface temperature, temperature depression (difference between air and dew point temperatures), radiation fluxes, and wind speed.

The province of Istanbul is located between two water bodies with different heat contents, and the Bosporus Strait that connects them causes currents to occur along the shorelines of the province. These features affect the formation, duration, and intensity of fog events in Istanbul. Because of its adverse impacts on aviation and navigation, it is important to study and understand the types and seasonal distribution of fogs forming in Istanbul and the effect of sea surface temperature on the occurrence, strength, and duration of fog over the surface. There are few studies on fog events in Istanbul. One study (Ozdemir et al. 2016) provides information about fog climatology at Ataturk Airport using 10-year (2006–2015) METAR data. It reports that radiation fog (about 59%) and advection fog (about 37%) are the most common types in 49 foggy days. It also reveals that the occurrence of fog is high in winter (49%) and fall (31%), while it is low in summer (2%) and spring (18%). To our knowledge, there is no study on fog modeling for Istanbul, an emerging aviation hub in the world. The objective of the present research is to evaluate, through sensitivity simulations, the performance of the WRF model in simulating a dense advection fog that occurred in Istanbul on February 19, 2014. Sensitivity simulations involve various model configurations, including different microphysics and PBL schemes and different initial and boundary conditions.

The manuscript is organized as follows: Sect. 2 presents the synoptic conditions and observations on February 19, 2014, Sect. 3 describes the data and meteorological model, Sect. 4 presents the evaluation of the sensitivity simulations, and finally, Sect. 5 provides a discussion and conclusions of the research.

2 Data and methodology

2.1 Site description and observation data

The province of Istanbul, located in the northwest of Turkey, is surrounded by the Black Sea in the north and the Sea of Marmara in the south. It is one of the metropolitan cities with a population of over 15 million. There are three major airports in the province. New Istanbul airport started to operate in 2019, which is later than the date of the case (February

19, 2014) considered in this study. The other two, Ataturk and Sabiha Gokcen (see Fig. 2 for locations), were open for national and international flights on that day. METAR (Meteorological Terminal Air Report) data belonging to these two airports and available sounding and meteorological station data in the province are used for the model evaluation. The 1-km spatial resolution corrected reflectance and cloud water path datasets from MODIS (moderate resolution imaging spectroradiometer) on Aqua and Terra are also used for the evaluation. Satellite data are available only at 08:35 a.m. (Terra) and 11:55 a.m. (Aqua).

2.2 Synoptic conditions

Istanbul experienced continual fog events between February 18 and 20, 2014, with the heaviest on the 19th under a persistent high-pressure system. At 0000 UTC on February 19, 2014, the high-pressure system with higher than 1025 hPa means sea level pressure prevails over the city of Istanbul (Fig. 1a). The city is also subject to relatively warm and humid air transferred from over the cooler Sea of Marmara by the southerly airflow at 0000 UTC (Fig. 1b). Despite weakening slightly, high pressure with weak southwesterly winds persists until the following day, continuing to transfer warm and moist air to over Istanbul (Figs. 1c and d). These synoptic conditions are conducive to the development of an advection fog over the city.

Meteorological reports represent that observers recorded mist (e.g., horizontal visibility not reduced below 1 km) late at night on February 18, and either mist or fog was observed at three stations (Sariyer, Kumkoy, and Bolge, whose locations are given in Fig. 3) on February 19, 2014. As METAR data point out, the fog begins to form at 1400 UTC and 1500 UTC at Ataturk and Sabiha Gokcen, respectively, on February 19, and it persists until early morning on February 20 at both airports. Figure 2 shows the diurnal cycle of temperature depression, visibility, wind speed, and wind directions at these airports for February 19. Surface air temperature approaches the dew point temperature at Ataturk Airport starting from midnight (Fig. 2a). Thus, the
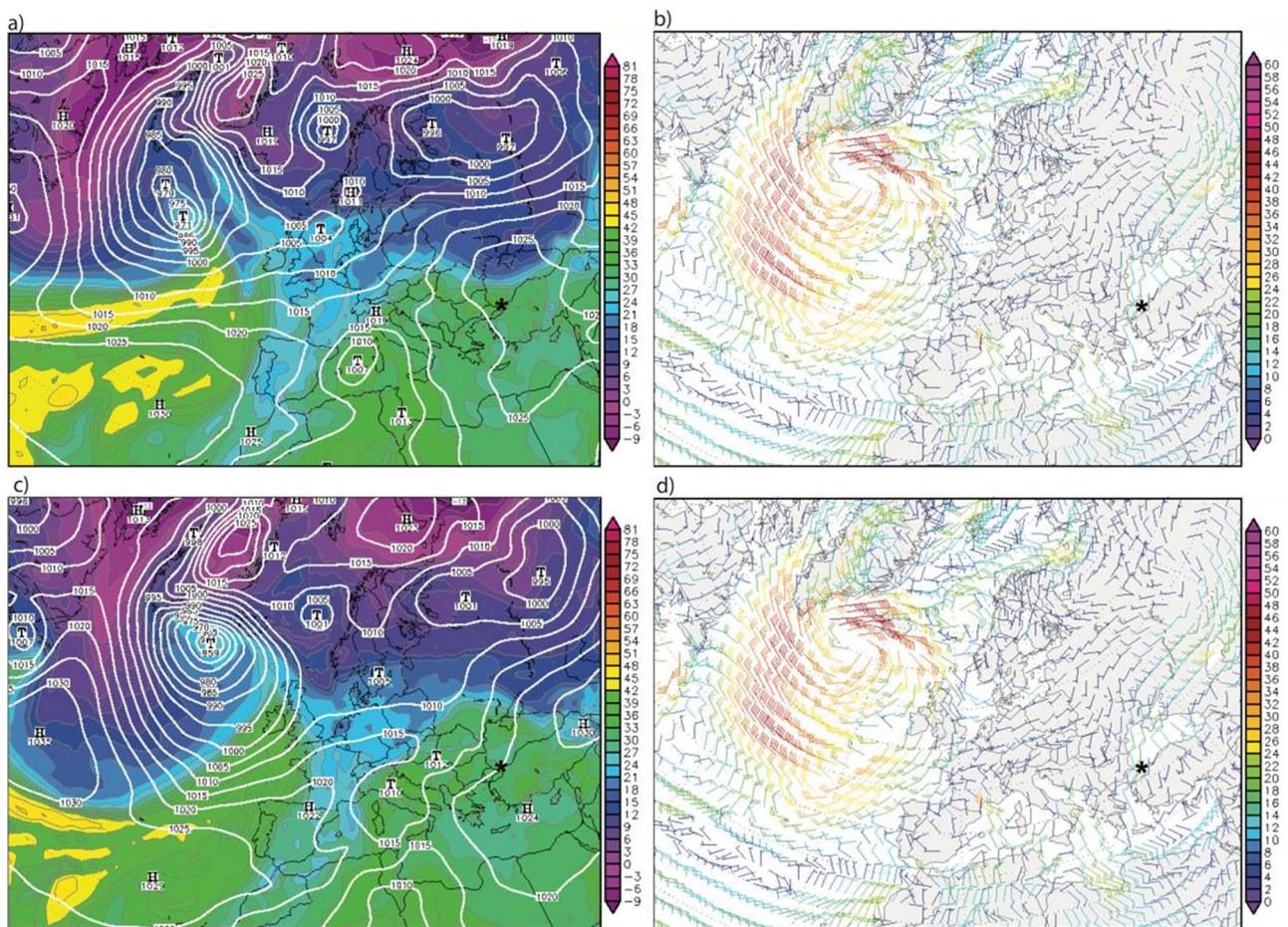

Fig. 1 Synoptic conditions on February 19, 2014. (**a** and **c**) Pseudo-potential temperature at 850 hPa (shaded) and mean sea level pressure (contour) at 0000 and 1800 UTC, respectively (**b** and **d**) 10-m wind speed (knot) at 0000 and 1800 UTC, respectively. Black asterisks show the location of Istanbul
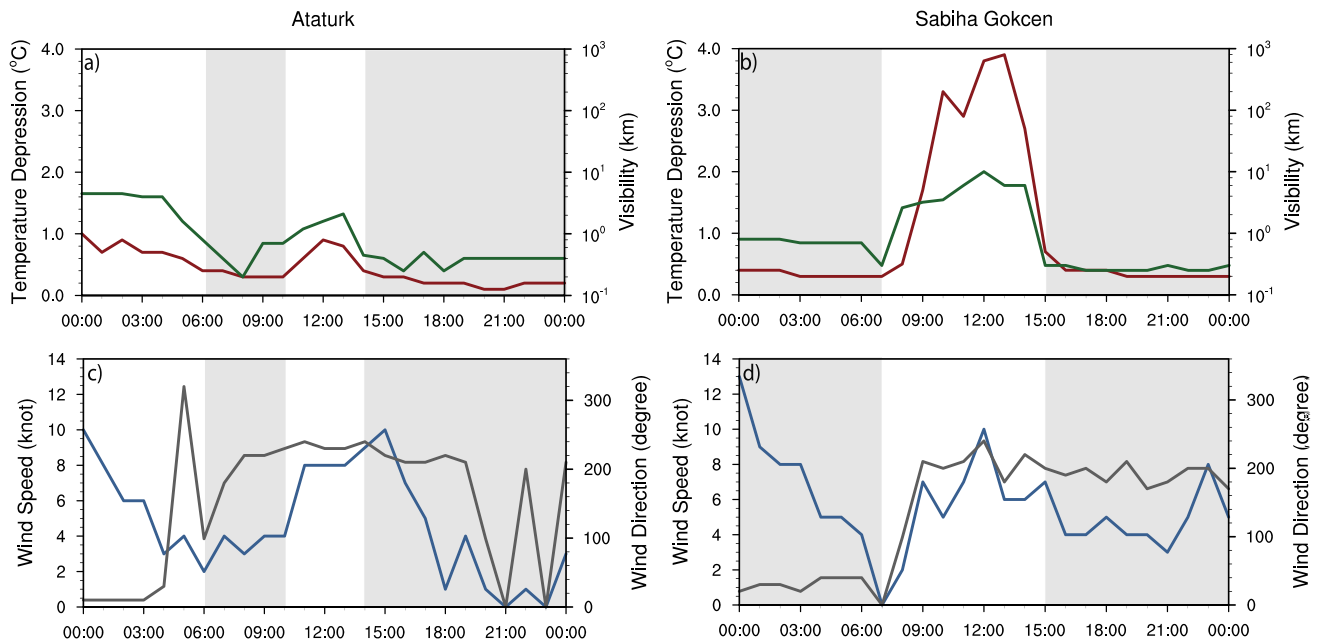
Fig. 2 Observations between February 19, 2014, 0000 and February 20, 2014, 0000 UTC from the METAR data at Ataturk (left) and Sabiha Gokcen (right) airports. **a** and **b** Visibility (green line) and temperature depression (red line) and **c** and **d** wind speed (blue line) and wind direction (gray line)
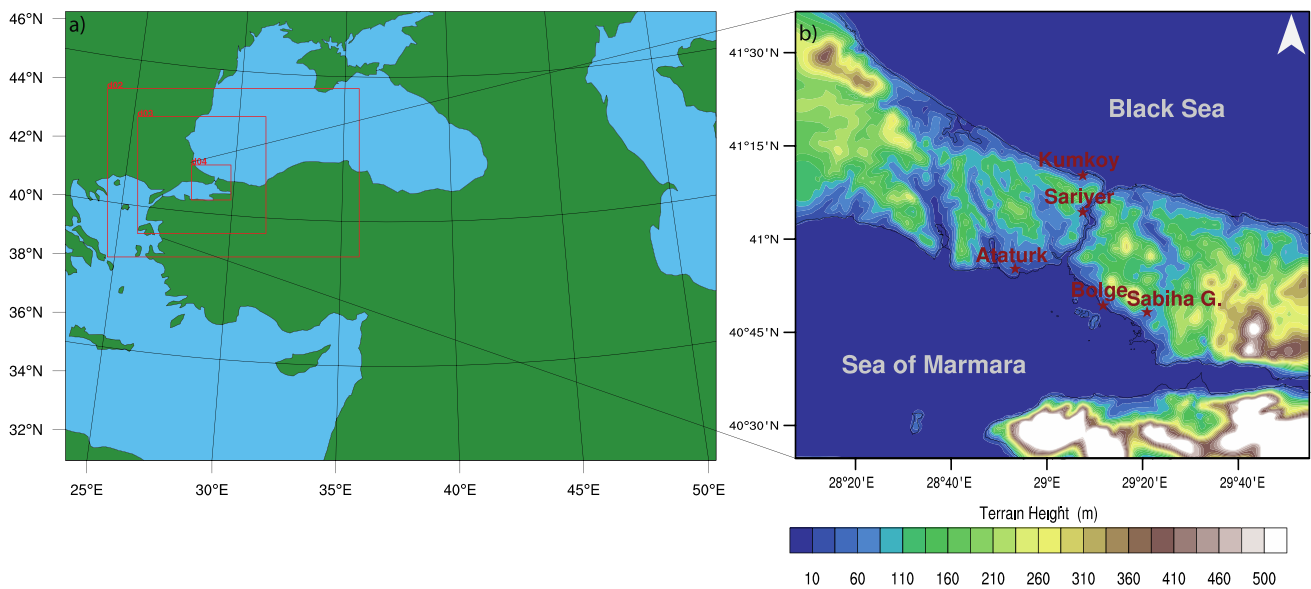
Fig. 3 Model domain configuration and innermost domain terrain height with observation sites

temperature depression, which is about 1 °C at midnight, shows a decreasing trend during the day, except a brief rise at around noon. In consistent with this variation, visibility decreases sharply early morning and becomes as low as 200 m at 0800 UTC, indicating the presence of fog. It increases gradually in response to increasing temperature depression until about 1300 UTC when it makes another

sharp drop to the levels below 500 m and remains at these levels for the rest of the day. The observations further show that the winds at this airport are northerly until early morning when they turn and remain mostly southerly during the rest of the day, and wind speed is below 3 knots during the low visibility hours (Fig. 2c). At Sabiha Gokcen Airport, temperature depression is smaller than 0.6 °C before 0800

UTC and after about 1500 UTC, and therefore the visibility is low (below 400 m early morning and below 200 m in the afternoon) at these times of the day, indicating the presence of fog (Fig. 2b). The changes in wind direction at this airport are in general similar to those at Ataturk Airport. Figure 2d indicates that the low wind speed helps to maintain low visibility. However, the wind is generally stronger at Sabiha Gokcen Airport than Ataturk Airport (Figs. 2c and d). The type of fog event on this day is identified as advection fog using the classification flowchart by Tardif and Rasmussen (2007).

## 2.3 Model setup and sensitivity simulations

In this study, we used the state-of-the-art WRF model (version 3.9.1) with one of the dynamical solvers, the Advanced Research WRF (ARW). The model is a well-known and widely used non-hydrostatic mesoscale atmospheric model (Skamarock et al. 2008). The model configuration involves four nested domains, and the number of horizontal grids from outermost to innermost domains are 94×65, 109×73, 166×151, and 154×136, and spatial resolutions 27 km (D01), 9 km (D02), 3 km (D03), and 1 km (D04), respectively (Fig. 3a). Model outputs for the innermost domain (D04) were used in all analyses of the study. The simulations are conducted with 61 vertical levels, 21 of which are located below 1.5 km. There are 10 levels between surface and 300-m height. The model top is set to 50 hPa. The simulation period is 36 h (February 18, 1200 UTC–February 20, 0000 UTC, 2014), and the first 6 h are considered the spin-up time. Initial and boundary conditions are mainly provided using the European Center for Medium-Range Weather Forecasts (ECMWF) reanalysis ERA-Interim data (Dee et al. 2011). The horizontal grid resolution of the ERA-Interim data is $0.75 \times 0.75°$, and the vertical resolution is 37 levels. The data are available at 6-h intervals. The WRF model comes with terrestrial datasets, and in our simulations, we used the 21-class MODIS-derived land use/land cover data and 30 arc-second USGS topography data. NOAH land surface model is set to simulate the land surface processes. For the sensitivity simulations on the initial and boundary conditions, additional forcing data are provided using $1 \times 1°$ National Center for Environmental Prediction (NCEP) FNL (Final) Operational Global Analysis and $0.3 \times 0.3°$ ECMWF ERA5 datasets. In addition to these datasets, in one of the sensitivity simulations, we forced the model with quarter degree horizontal resolution Optimum Interpolation Sea Surface Temperature (OISST) data provided by National Oceanic and Atmospheric Administration (NOAA). Sensitivity simulations are conducted in two groups: one for the physics options (i.e., microphysics, PBL, cumulus, and radiation schemes) and one for the non-physics options (i.e., different initial-boundary conditions and SST).

2.3.1 Sensitivity to physics options

We adopted a hierarchical approach in determining the sensitivity of fog simulation to physics options. Microphysics parameterization is very important for fog prediction. Therefore, we first focused on exploring the sensitivity to available microphysics parameterizations by keeping everything else the same (e.g., PBL, surface layer, cumulus, and radiation parameterizations) in the model. The Mellor–Yamada–Nakanishi–Niino (MYNN) 2.5-level parametrization (Nakanishi and Niino 2004) was used for the PBL by Roman Cascon et al. (2012) to be effective for simulating fog conditions. Moreover, Hahmann et al. (2020) indicated that MYNN2.5 performs well over the region of interest in the present study. The Kain-Fritsch cumulus scheme (Kain 2004) is a widely used cumulus parametrization set for this sensitivity experiment with RRTMG short and long-wave radiation schemes (Iacono et al. 2008). Six available microphysics schemes (MP) from single to double moment parameterizations, WSM6 (Hong and Lim 2006), Morisson (Morrison et al. 2009), NSSL (Mansell et al. 2010), NSSL with cloud condensation nuclei (CCN), Thompson (Thompson and Eidhammer 2014), and Milbrandt (Milbrandt and Yau 2005a, b), available in the WRF model were tested to explore the performance of the microphysics schemes in the simulation of the fog episode. Hydrometeors are important for the computation of radiative transfer, especially for overcast weather conditions. Cloud, rain, snow, ice, and graupel droplets, are hydrometeors considered in the model microphysics schemes. However, hail droplets are taken into account in NNSL and Milbrandt schemes used in this study. Except for WSM6, all microphysics schemes are double-moment, which means they predict a number of concentrations of each species. Milbrandt, one of the most complex and more time-consuming parametrizations in all microphysics schemes, has commonly been used in fog prediction (e.g., Gultepe et al. 2015; Steenveld and Bode 2018) and extreme weather studies, such as hail storm, heavy rain, etc. (e.g., Toker et al. 2020; Zhou et al. 2020).

In the next stage, we evaluated the sensitivity to cumulus schemes (CU) considering the Tiedtke scheme (Tiedtke 1989; Zhang et al. 2011) in addition to KF. In these simulations, we used radiation schemes as in MP sensitivity simulations. The microphysics scheme whose performance was comparatively better than the others in MP sensitivity, Milbrandt, was used in the CU sensitivity simulations.

In the third and fourth stages, we assessed the sensitivity to PBL and radiation schemes, respectively, in a similar manner to that in the second stage. Namely, our setup contained Milbrandt microphysics, RRTMG radiation, and Tiedtke cumulus schemes for PBL sensitivity experiments. Although microphysical processes affect the radiative balance due to the cloud cover and play a crucial role
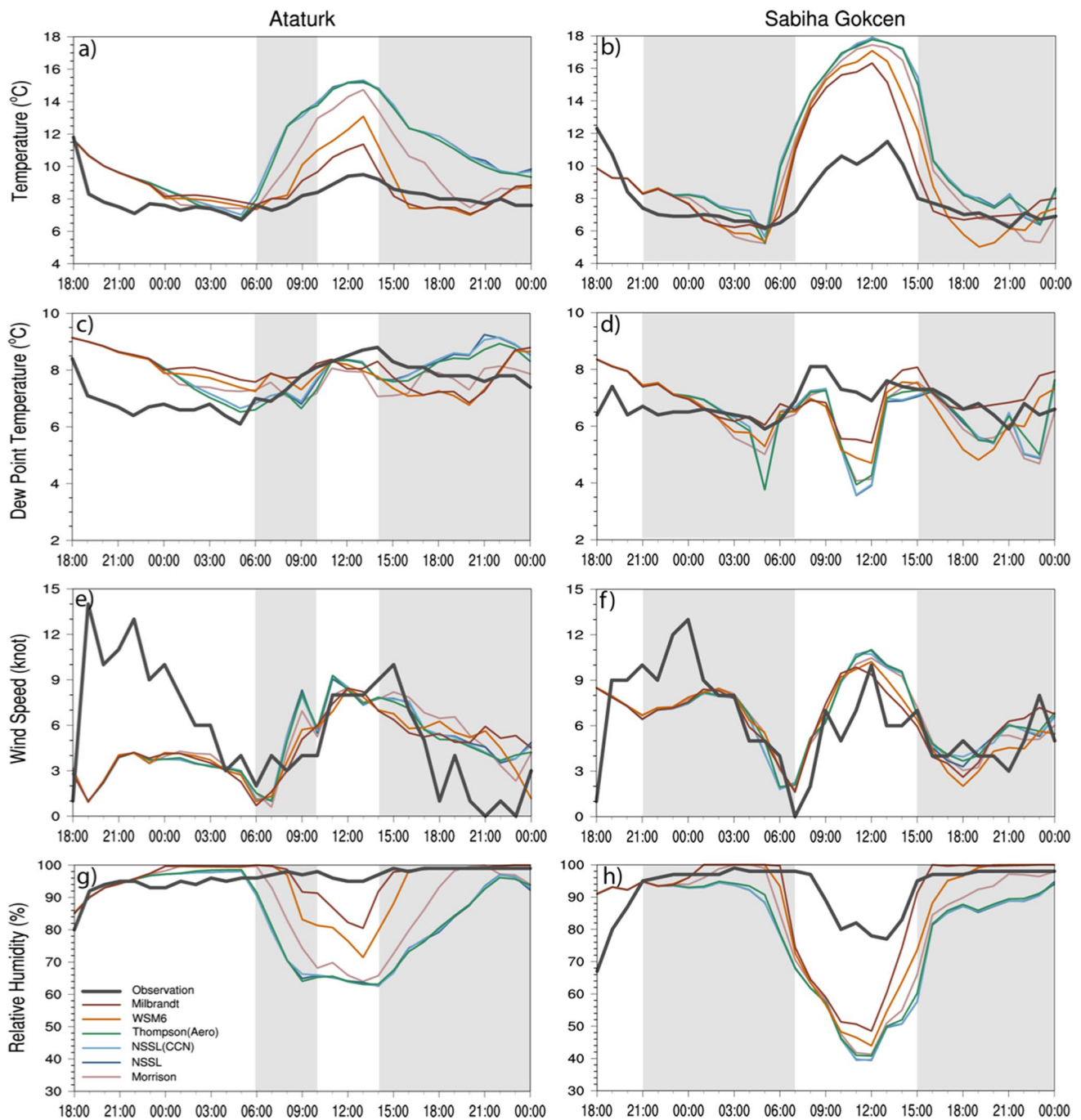
Fig. 4 Results of the microphysics sensitivity experiment. Observed and modeled temperature (**a** and **b**), dew point temperature (**c** and **d**), wind speed (**e** and **f**), and relative humidity (**g** and **h**) at Ataturk (left column) and Sabiha Gokcen (right column) airports

in continuity and dissipation processes, planetary boundary layer processes are important for the formation of fog (Steenveld et al. 2015). In the PBL sensitivity, six different local and non-local PBL schemes used widely for fog simulations were tested: MYNN2.5 (Nakanishi and Niino 2006), MYNN3 (Nakanishi and Niino 2006), MYJ (Janjic 1994), BouLac (Bougeault and Lacarrere 1989), ACM2 (Pleim 2007), and YSU (Hong et al. 2006).

Finally, we performed additional simulations for both shortwave and longwave radiation schemes together with the outperformed PBL scheme obtained from the PBL sensitivity simulations to find the better performing radiation schemes consistent with the radiation balance. Therefore, RRTMG and RRTMG-fast schemes were used for testing the model sensitivity to shortwave radiation parameterization, and additional simulations were carried out for longwave

radiation and shortwave radiation schemes, namely RRTM (Mlawer et al. 1997) and Dudhia (Dudhia 1989), respectively. In the evaluation part, we aimed to determine the physics parameterizations that reproduce comparatively better diurnal cycles of the meteorological variables, especially air and dewpoint temperatures. Hence, in this study, we tested most of the available physics options of the WRF model, which are deemed important in fog processes, in a hierarchic manner to find a parameterization combination that results in improved simulation of a dense fog episode in Istanbul. A similar approach for different sensitivities was also applied by Pithani et al. (2019b).

2.3.2 Sensitivity to initial and boundary conditions

In addition to the model's sensitivity to physics parameterizations, we investigated the effects of initial and boundary conditions (IC-BC) in the simulation of the dense fog episode in Istanbul. For this purpose, we forced the model with different boundary conditions, including also a different SST dataset. ERA-Interim reanalysis was used as the main IC-BC input to the model. The model was also forced with ERA5 and FNL data to see whether the use of different IC-BC datasets improved the prediction of the fog event. By default, the model receives surface boundary conditions over sea through skin temperature in the physics sensitivity simulations. Istanbul sits next to two major water bodies, and therefore the surface boundary conditions of the water bodies could be important for the prediction of the advection fog. Thus, we forced the model with OISST data in the additional sensitivity simulations. Table 1 gives a summary

of the sensitivity simulations involving the physics options and initial and boundary conditions.

3 Results

3.1 Assessment of sensitivity to physics options

Performance of the WRF model was evaluated against observed temperature, dew point temperature, relative humidity at 2 m height, wind speed at 10 m height, and vertical changes of temperature depression, equivalent potential temperature, mixing ratio, and wind speed for the dense fog episode.

3.1.1 Microphysics sensitivity

A comparison between six different microphysics simulations and observations is given in Fig. 4. The model with all microphysics schemes simulated a realistic diurnal cycle for the near-surface temperature, however, none of the simulations captured well the temperature variation between 06:00 a.m. and 15:00 p.m. when it indicated both fog and mist episodes recorded by the observer. The model overestimated the temperature at both airports during this period, but the overestimation was substantially higher at Sabiha Gokcen Airport. This warm bias could cause rapid dissipation of the modeled fog. Temperature plots further illustrate that the Milbrandt microphysics scheme performed comparatively better than the other schemes. In general, the model with all MPs tended to produce a moister air early in the morning

Table 1 Summary of the sensitivity simulations

Experiment name	IC/BC	Microphysics	Cumulus	PBL	Short-wave radiation	Long-wave radiation
WSM6	ERAINT	WSM6	KF	MYNN2.5	RRTMG	RRTMG
Milbrandt		Milbrandt	KF	MYNN2.5	RRTMG	RRTMG
Morisson		Morisson	KF	MYNN2.5	RRTMG	RRTMG
NSSL		NSSL	KF	MYNN2.5	RRTMG	RRTMG
NSSL-CCN		NSSL-CCN	KF	MYNN2.5	RRTMG	RRTMG
Thompson-aerosol		Thompson-AER	KF	MYNN2.5	RRTMG	RRTMG
MYNN2.5-KF	ERAINT	Milbrandt	KF	MYNN2.5	RRTMG	RRTMG
MYNN2.5-Tiedtke		Milbrandt	Tiedtke	MYNN2.5	RRTMG	RRTMG
ACM2	ERAINT	Milbrandt	Tiedtke	ACM2	RRTMG	RRTMG
BouLac		Milbrandt	Tiedtke	BouLac	RRTMG	RRTMG
MYJ		Milbrandt	Tiedtke	MYJ	RRTMG	RRTMG
MYNN2.5		Milbrandt	Tiedtke	MYNN2.5	RRTMG	RRTMG
MYNN3		Milbrandt	Tiedtke	MYNN3	RRTMG	RRTMG
YSU		Milbrandt	Tiedtke	YSU	RRTMG	RRTMG
YSU	ERAINT	Milbrandt	Tiedtke	YSU	RRTMG-fast	RRTMG
YSU-SW24-LW1		Milbrandt	Tiedtke	YSU	RRTMG-fast	RRTM
YSU-SW1-LW1		Milbrandt	Tiedtke	YSU	Dudhia	RRTM
YSU-SW1-LW1-OISST	ERAINT-OISST	Milbrandt	Tiedtke	YSU	Dudhia	RRTM
ERA5	ERA5	Milbrandt	Tiedtke	YSU	Dudhia	RRTM
FNL	FNL	Milbrandt	Tiedtke	YSU	Dudhia	RRTM

and late at night, and a drier air during the daytime than the observations at both airports (Figs. 4c and d). Wind speed variations were simulated fairly well by the model with different MPs; however, the strong winds of early morning hours were substantially underestimated, especially at Ataturk Airport (Figs. 4e and f). For relative humidity at the surface, a high negative bias was evident during the daytime for both airports (Figs. 4g and h).

Error statistics for the MP sensitivities were calculated for the simulation period at Ataturk and Sabiha Gokcen stations to reveal the performance of the model with each MP and to identify the better performing microphysics scheme to use in the following sensitivity simulations. Table 2 gives the mean bias (MB) and root mean square error (RMSE) statistics for temperature (T), dew point temperature (Td), wind speed (wsp), and relative humidity (RH) at Ataturk and Sabiha Gokcen airports. Milbrandt microphysics produced comparatively better MB and RMSE values for the temperature at Ataturk (0.7 and 1.2 °C, respectively) and at Sabiha Gokcen (1.3 and 2.5 °C, respectively) airports. Its performance was better in dew point temperature and relative humidity statistics, and more or less equivalent to the others in wind speed statistics.

Table 2 Error statistics for the sensitivity simulations involving microphysics schemes at Ataturk and Sabiha Gokcen airports for the 30-h simulation period

Simulation	Variable	Sabiha Gokcen		Ataturk	
		MB	RMSE	MB	RMSE
WSM6	T (°C)	1.31	2.99	0.94	1.54
	Td (°C)	−0.32	1.11	0.43	1.12
	wsp (knot)	0.04	2.52	−1.29	4.35
	RH (%)	−7.0	17.0	−2.0	8.0
Milbrandt	T (°C)	1.25	2.5	0.71	1.18
	Td (°C)	0.13	0.89	0.56	1.15
	wsp (knot)	0.2	2.56	−1.21	4.41
	RH (%)	−4.0	14.0	−0.2	5.0
Morrison	T (°C)	1.74	3.39	1.74	2.38
	Td (°C)	−0.44	1.19	0.34	1.05
	wsp (knot)	0.29	2.62	−0.99	4.29
	RH (%)	−10.0	18.0	−7.0	14.0
NSSL	T (°C)	2.47	3.76	2.8	3.39
	Td (°C)	−0.38	1.28	0.6	1.09
	wsp (knot)	0.3	2.76	−1.02	4.35
	RH (%)	−13.0	21.0	−12.1	18.0
NSSL-CCN	T (°C)	2.48	3.77	2.79	3.38
	Td (°C)	−0.37	1.27	0.6	1.09
	wsp (knot)	0.32	2.74	−1.03	4.33
	RH (%)	−13.0	20.0	−11.0	18.0
Thompson-aerosol	T (°C)	2.4	3.69	2.68	3.31
	Td (°C)	−0.34	1.19	0.49	1.05
	wsp (knot)	0.39	2.74	−1.08	4.32
	RH (%)	−13.0	20.0	−11.0	18.0

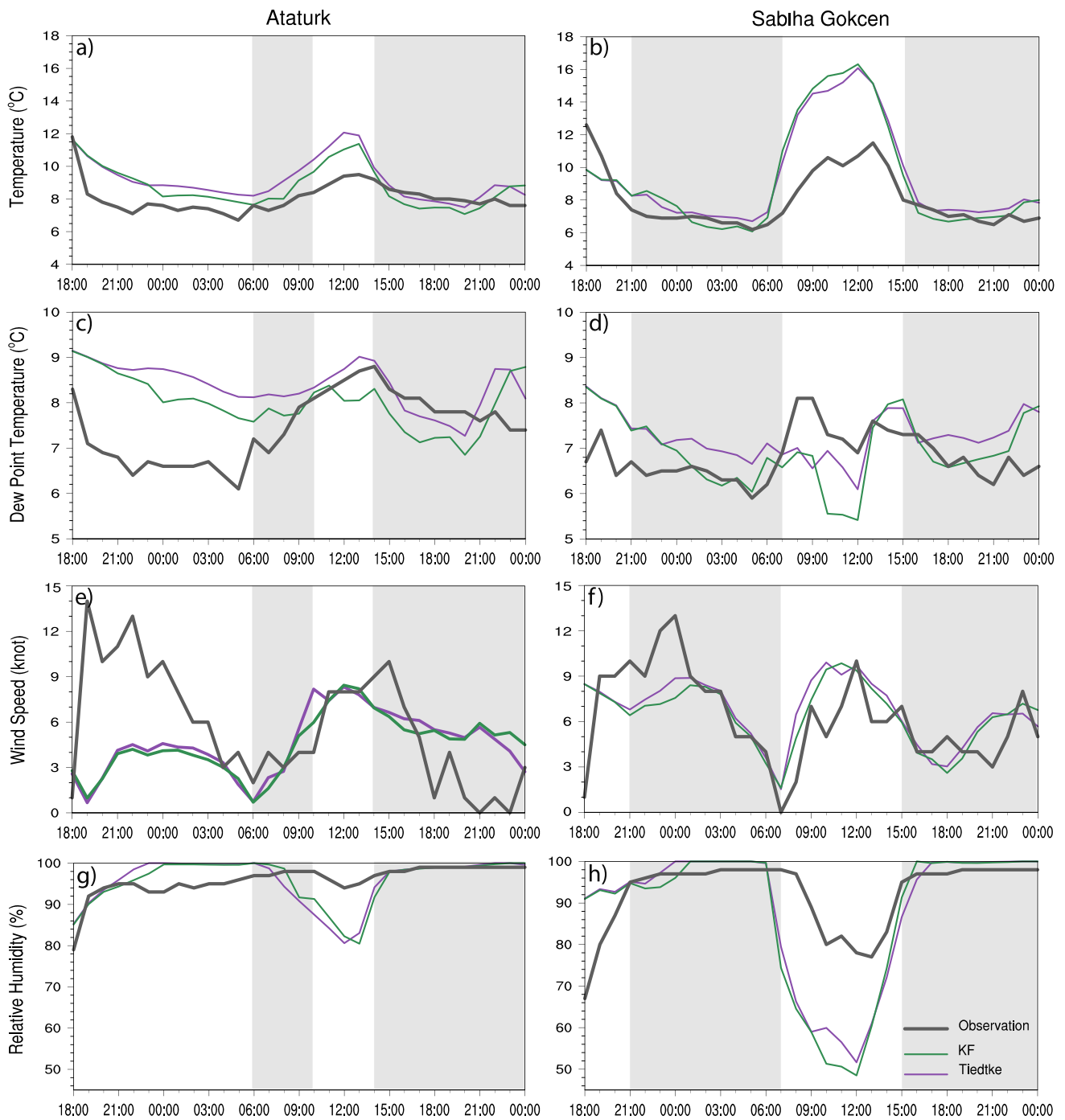T, temperature; Td, dew point temperature; *wsp*, wind speed; *RH*, relative humidity.

3.1.2 Cumulus sensitivity results

The first group of simulations demonstrated that the model has a warm bias, especially during the daytime. Diurnal temperature and dew point variations showed that the model rapidly warms the air right after sunrise, especially at Sabiha Gokcen Airport, which is inland. In another sensitivity test, we investigated the effect of the cumulus parameterization on the surface variables by switching from Kain-Fritsch (KF) to Tiedtke in the model. Figure 5 shows the diurnal variations of temperature, dew point temperature, wind speed, and relative humidity at Ataturk and Sabiha Gokcen airports. Changing the cumulus scheme did not make any significant alteration in the diurnal variations of the variables. The performance of the Tiedtke scheme in near-surface temperature simulation was worse than that of KF at Ataturk station (Fig. 5a). The use of the Tiedtke scheme does not yield an overall improvement of the dew point temperature estimation over the use of KF. It seems to improve dew point temperature simulation during the daytime while degrading it during the nighttime (Figs. 5c and d). The Tiedtke scheme did not make noteworthy changes in the wind speed simulations over the KF scheme (Figs. 5e and f). Both schemes produced fairly similar performances in the estimation of relative humidity (Figs. 5g and h). These simulations indicated that the Tiedtke scheme did not make an overall improvement over the KF scheme in terms of the reproduction of surface variables. Nevertheless, we decided to continue with the Tiedtke scheme due to its comparatively better performance at around noon, when model performance is to be more problematic in this sensitivity study.

3.1.3 PBL sensitivity

Fog development is primarily governed both by the PBL processes which initiate the fog formation and the microphysical processes that play a controlling role in the dissipation of fog in a model (Steeneveld et al. 2015). There are many options for these schemes in the model, and therefore it is difficult to decide on a scheme combination which would produce better performance in fog development without testing the model for different combinations. Previous studies on this subject may also play a guiding role in the selection process. Many studies have investigated the performance of local and non-local PBL schemes in fog prediction (e.g., Román-Cascón et al. 2012; Payra and Mohan 2014; Steeneveld et al. 2015; Chaouch et al. 2017; Pithani et al. 2019a). Steeneveld et al. (2015) and Payra and Mohan (2014) showed that non-local (e.g., YSU and ACM2) PBL schemes predict fog onset fairly well. However, other studies
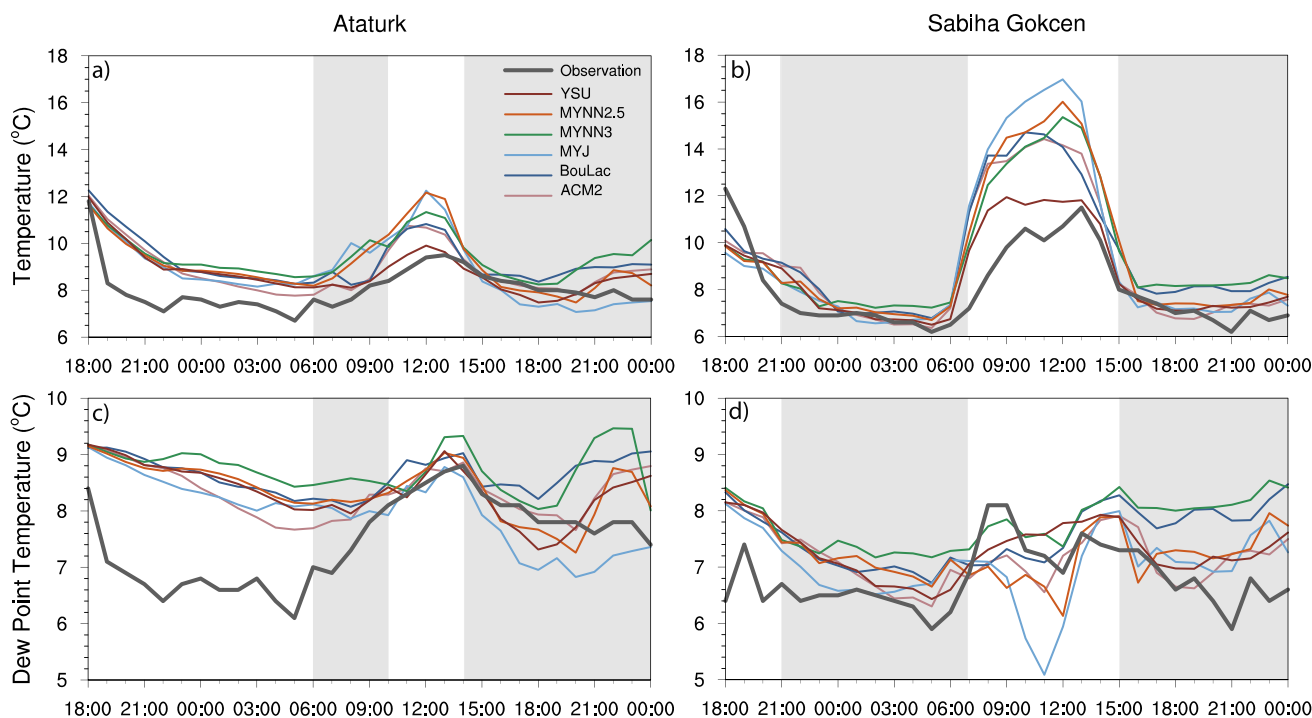
Fig. 5 Results of the cumulus sensitivity experiment. Observed and modeled temperature (**a** and **b**), dew point temperature (**c** and **d**), wind speed (**e** and **f**), and relative humidity (**g** and **h**) at Ataturk (left column) and Sabiha Gokcen (right column) airports

indicated that local PBL schemes simulated a complete fog life cycle (e.g., Román-Cascón et al. 2012; Chaouch et al. 2017; Pithani et al. 2019a).

In the present study, we tested both local (MYNN2.5, MYNN3, MYJ, and BouLac) and non-local (ACM2 and YSU) PBL schemes. These sensitivity tests were conducted using Milbrandt microphysics and Tiedtke cumulus schemes

and the same long-wave and short-wave radiation schemes (RRTMG) as in MP simulations. Figure 6 shows the diurnal temperature and dew point temperature variations for the selected PBL schemes. The near-surface temperature was overestimated by the model with all PBL schemes during the fog event at Ataturk Airport while it was consistent with the observations at Sabiha Gokcen Airport. However,
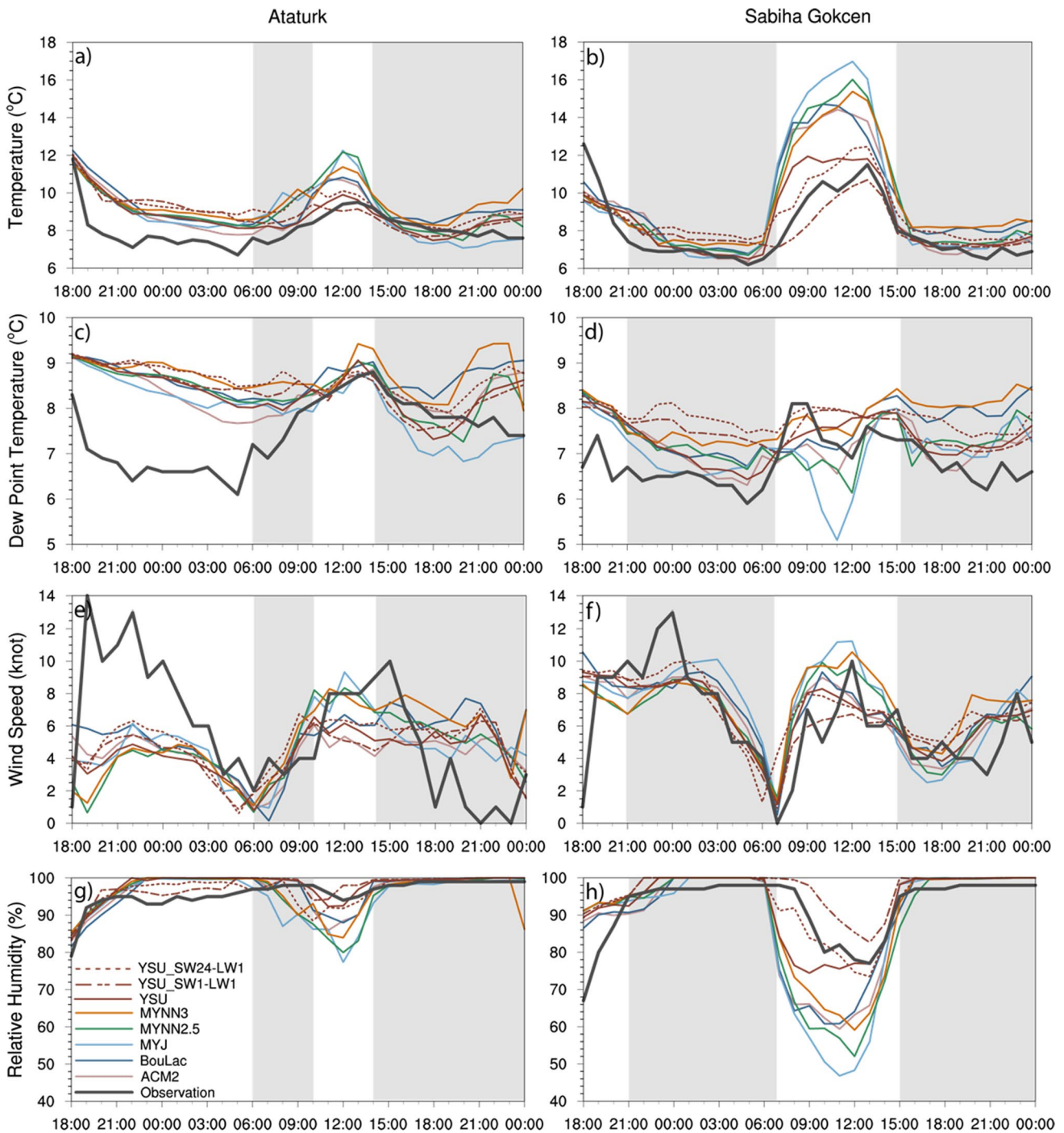
Fig. 6 Results of the PBL sensitivity experiment. Observed and modeled temperature (**a** and **b**) and dew point temperature (**c** and **d**) at Ataturk (left column) and Sabiha Gokcen (right column) airports

the overestimation was more obvious after the fog gradually dissipated between 1000 and 1300 UTC for Ataturk and between 0800 and 1400 UTC for Sabiha Gokcen. This warm bias can reach up to 7 and 5 °C for Sabiha Gokcen and Ataturk airports, respectively, depending on the PBL scheme (Fig. 6a and b). The modeled dew point temperatures were also higher than the observations at Ataturk Airport (about 2 °C) before 0900 UTC on February 19. The deviations were relatively small for the rest of the day at Ataturk Airport and for the entire day at Sabiha Gokcen Airport.

The model was inclined to produce a warm bias at around noon at both stations. Because this is somewhat a common pattern in all PBL simulations, we decided to examine the effect of the shortwave radiation scheme on surface variables by conducting further simulations with the optimized version of the RRTMG short-wave radiation, namely RRTMG-fast. Figure 7 exhibits the results of each PBL simulation with an RRTMG-fast radiation scheme. Changing the shortwave radiation scheme from RRTMG to RRTMG-fast produced relatively small changes in air and dew point temperature simulations at Ataturk Airport (Figs. 6a and 7a). However, the use of RRTMG-fast short-wave radiation with the non-local YSU PBL scheme greatly improved temperature simulation at Sabiha Gokcen (Figs. 6b and 7b). The dew point temperature pattern in this simulation was almost similar to that in the RRTMG simulation at Ataturk. However, its variation around noon followed the observation better than

that of RRTMG. Still, these settings did not fix the warm bias for early morning and late afternoon at either station (Figs. 7c,d). The model with all different schemes deviated from the wind speed observations significantly during the nighttime at Ataturk Airport, however, it captured the variation during the daytime fairly well (Fig. 7e). The model did a better job in reproducing the wind variation at Sabiha Gokcen Airport (Fig. 7f).

The model with different PBL schemes in general well simulated RH at both stations, however, there was a tendency to underestimate it at around noon and overestimate at the other times of the day (Figs. 7g–h). It seemed that the simulation, including YSU as the PBL scheme, gave a comparatively better RH match with the observations than the others. This is especially true for the midday simulations. Considering the improvement in the simulated temperature, dew point temperature, and relative humidity due to alteration of the short-wave radiation scheme, i.e., from RRTM to RRTMG-fast, in the YSU simulation, we conducted two more simulations involving other short-wave and long-wave schemes available in the model. Thus, in one case, we performed a WRF simulation with the settings of Milbrandt microphysics, YSU PBL, Tiedtke cumulus, and RRTMG-fast shortwave together with RRTM long-wave scheme (named as YSU-SW24-LW1). In another case, we carried out a simulation by changing the short-wave radiation RRTMG-fast to Dudhia with

Fig. 7 Sensitivity simulation results of PBL scheme and results of radiation scheme for YSU PBL scheme. Temperature (**a** and **b**), dew point temperature (**c** and **d**), wind speed (**e** and **f**), and relative humidity (**g** and **h**) at Ataturk (left column) and Sabiha Gokcen (right column) airports

RRTM long-wave scheme (named as YSU-SW1-LW1). These radiation schemes seem to improve simulations at around noon at the expense of other times.

T, temperature; *Td*, dew point temperature; *T-Td*, temperature depression; *wsp*, wind speed; *RH*, relative humidity.

We calculated error statistics for both entire simulation periods and only recorded fog hours at two sites (Table 3). In general, the performance of the model is fairly well, however, it is better at Ataturk Airport than Sabiha Gokcen. The simulations with the YSU scheme come out with lower error statistics than the others. RMSE (MB) values for

Table 3 Error statistics for PBL/radiation sensitivity simulations at Sabiha Gokcen and Ataturk airports for the 30-h simulation period and only fog hours

Simulation	Variable	Sabiha Gokcen				Ataturk			
		30-h		fog-hour		30-h		fog-hour	
		MB	RMSE	MB	RMSE	MB	RMSE	MB	RMSE
ACM2	T (°C)	1.05	1.99	0.55	1.14	0.87	1.16	0.45	0.67
	Td (°C)	0.35	0.69	0.45	0.59	0.89	1.17	0.44	0.64
	$T - Td$ (°C)	0.7	2.21	0.14	1.08	1.32	2.98	0.01	0.3
	Wsp (knot)	0.48	2.43	−0.29	1.81	−1.42	4.01	0.53	3.13
	RH (%)	−3.0	11.0	0	6.3	1 0.0	4.0	0.69	2.17
BouLac	T (°C)	1.42 0.74	2.13	1.08	1.39	1.19	1.41	0.79	0.95
	Td (°C)	0.68	1.0	0.94	1.05	1.19	1.39	0.79	0.92
	$T - Td$ (°C)	0.82	2.16	0.19	1.02	1.3	2.89	0.0	0.31
	Wsp (knot)	−3.0	2.67	0.07	1.97	−0.5	3.94	1.68	3.7
	RH (%)		11.0	−0.28	6.07	1.0	4.0	0.69	2.19
MYJ	T (°C)	1.36	2.72	0.54	1.1	0.83	1.38	0.23	1.06
	Td (°C)	0.2	0.85	0.46	0.59	0.54	1.16	−0.21	0.65
	$T - Td$ (°C)	1.16	3.26	0.13	1.02	1.78	4.13	0.45	0.78
	Wsp (knot)	1.05	2.78	−0.09	2.13	−0.94	3.76	0.91	2.94
	RH (%)	−4.0	15.0	0.06	6.04	−1.0	6.0	−2.44	4.68
MYNN2.5	T (°C)	1.35	2.32	0.73	1.05	1.1	1.42	0.59	0.94
	Td (°C)	0.43	0.85	0.63	0.76	0.94	1.3	0.35	0.67
	$T - Td$ (°C)	0.92	2.64	0.15	0.88	1.53	3.49	0.24	0.59
	wsp(knot)	0.45	2.51	−0.47	1.99	−1.1	4.34	1.31	3.0
	RH (%)	−4.0	13.0	−0.06	5.29	−0.1	6.0	−0.94	3.54
MYNN3	T (°C)	1.47	2.14	1.08	1.23	1.4	1.57	1.14	1.35
	Td (°C)	0.96	1.12	1.15	1.23	1.29	1.53	0.87	1.06
	$T - Td$ (°C)	0.51	1.99	−0.04	0.61	1.12	2.83	0.27	0.67
	Wsp (knot)	1.0	2.81	−0.03	2.18	−0.7	4.39	2.05	3.41
	RH (%)	−2.0	10.0	1.06	4.02	0.0	5.0	−1.19	4.12
YSU	T (°C)	0.51	1.13	0.44	0.76	0.72	1.07	0.23	0.59
	Td (°C)	0.5	0.7	0.52	0.6	0.91	1.29	0.32	0.66
	$T - Td$ (°C)	0.01	1.29	−0.05	0.61	0.63	1.77	−0.08	0.15
	Wsp (knot)	0.46	2.33	−0.24	1.77	−1.4	4.2	0.73	3.26
	RH (%)	1.0	7.0	1.17	4.12	2.0	3.0	1.25	1.54
YSU-SW24-LW1	T (°C)	0.77	1.11	0.97	1.02	1.2	1.43	0.83	1.08
	Td (°C)	0.98	1.09	1.12	1.17	1.19	1.5	0.69	0.92
	$T - Td$ (°C)	−0.21	0.95	−0.14	0.38	0.41	1.46	−0.14	0.47
	Wsp (knot)	0.86	2.53	0.36	2.07	−0.77	3.86	1.53	3.31
	RH (%)	2.0	6.0	1.72	2.95	1.0	3.0	−0.25	2.92
YSU-SW1-LW1	T (°C)	0.04	0.93	0.52	0.66	0.83	1.28	0.29	0.67
	Td (°C)	0.7	0.86	0.78	0.87	0.97	1.37	0.37	0.72
	$T - Td$ (°C)	−0.66	1.08	−0.27	−0.31	−0.05	0.81	−0.08	0.23
	Wsp (knot)	0.21	2.23	−0.17	1.81	−1.27	4.08	1.05	3.35
	RH (%)	5.0	6.0	2.56	2.75	2.0	2.0	1.31	2.05

temperature using the YSU PBL scheme with different radiation schemes range from 0.93 (0.04) to 1.13 °C (0.77 °C) at Sabiha Gokcen for the entire simulation period. However, RMSE (MB) values for dew point temperature vary between 0.69 (0.2) and 0.86 °C (0.7 °C) for both non-local schemes (ACM2, YSU, and YSU-SW1-LW1) and local schemes (MYJ and MYNN2.5). RMSE (MB) values for temperature are between 1.07 (0.72) and 1.16 °C (0.83 °C) for ACM2, YSU, and YSU-SW1-LW1 at Ataturk Airport. Similar to the statistics for dew point temperature at Sabiha Gokcen, the local scheme MYJ has low RMSE and MB beside non-local PBL schemes (ACM2 and YSU) at Ataturk Airport. RMSE (MB) values are in the range from 1.16 (0.54) to

1.29 °C (0.94 °C) for the entire simulation time. These error statistics demonstrate that the model simulates the diurnal cycle of temperature fairly well. In line with temperature and dew point performance, the simulations with YSU PBL schemes produce low RMSE for dew point depression over the whole simulation period. Wind speed and relative humidity statistics are also in a reasonable range. In addition to the assessment of the performance over the entire simulation period, the performance of the sensitivity simulations during the fog events summarizes that those with the YSU PBL schemes comparatively well simulate the dew point depression, which defines the fog formation at both Ataturk (e.g., the YSU simulation) and Sabiha Gokcen airports

(e.g., the YSU-SW1-LW1 simulation). RMSE (MB) value is 0.15 °C (− 0.08 °C) at Ataturk and 0.31 °C (− 0.27 °C) at Sabiha Gokcen. Temperature, dew point temperature, wind speed, and relative humidity errors are lower during the fog period than during the entire simulation hours.

In order to understand the differences in the evolution of the modeled conditions between the PBL schemes, we examined the PBL height, relative humidity, potential temperature, and air advection. Figure 8 indicates that PBL height is below 500 m at Ataturk Airport for all schemes. The atmosphere is very stable during the fog hours, and RH is over 90% at the surface during the simulation period. PBL height is lower than 200 m for all PBL schemes except the local MYNN2.5 and MYNN3 schemes (Fig. 8). A warm-moist air advection at lower altitudes (below 200 m) at Ataturk airport for all PBL schemes except MYNN25 and MYNN3 in the morning hours is also evident (Figure S1). Cold air advection during the observed morning fog hours is more pronounced in the YSU-SW1-LW1 case (Figure S1h). All PBL schemes produced warm-moist air during the afternoon fog hours at Ataturk Airport, but the moist air advection in YSU-SW1-LW1 is stronger than the others (Figure S1h).

Stable atmospheric conditions are also evident at Sabiha Gokcen Airport during the simulation period (Fig. 9). RH is over 90% near the surface. PBL height at the airport is between 50 and 100 m for all non-local and local BouLac schemes during the morning and afternoon fog events (Fig. 9). Warm and moist air is advected at altitudes below 200 m at Sabiha Gokcen for all PBL schemes during the simulated morning fog event (Figure S2). Differences between the PBLs occur around noon (between morning dissipation and the afternoon onset) when all simulations show a warm and dry air advection except, YSU-SW1-LW1 (in Figure S2h), which affects the onset of the afternoon fog with a moist air advection. Forced convection is effective at around 250 m height at both Ataturk and Sabiha Gokcen airports during the morning fog, while free convection governs the presence and duration of the afternoon fog at the airports for all sensitivity simulations according to buoyancy and shear production calculations for these stations (Figures S3 and S4).

Figure 10 shows the spatial distribution of daily liquid water content (LWC) over the innermost domain for PBL and radiation sensitivity simulations. Here the simulations are compared with each other as there are no observed LWC data over the city. All simulations produce high LWC over the Sea of Marmara. Simulations such as BouLaC, MYNN2.5, YSU, YSU-SW1-LW1 (Figs. 10b, d, f, and h) also produce comparatively high LWC values over the Black Sea. MYJ simulation has lower LWC values over the domain (Fig. 10c), while the YSU simulation has high LWC (Fig. 10f). All simulations produce relatively high LWC along the Bosphorus. LWC increases up to 0.15–0.2 g/kg

over the Asian side of the city for the simulations except for YSU, whose LWC is around 0.25–0.30 g/kg. Figure 8h exhibits that simulated LWC by the YSU-SW1-LW1 falls between those of the YSU and the YSU-SW24-LW1. Therefore, the YSU-SW1-LW1 simulation does not produce as much cloud mixing ratio as the YSU (Fig. 10f), but it also does not produce LWC as low as that of the YSU-SW24-LW1 (Fig. 10g).

Sounding observations are available at Bolge station, whose location is very close to Sabiha Gokcen Airport. Weather reports at this station indicated mist early in the morning on February 19, 2014. Hence, we used 0000 UTC soundings to assess the performance of the simulations for the lowest one thousand meters of the troposphere. The comparison suggests that the simulations produce a moister surface air (below 300 m) than the observations. However, this first 300 m layer of the atmosphere is saturated and calmer compared to what the simulations produce. It could be said that the YSU simulation comparatively better captures the vertical profiles for the first few hundred meters (Fig. 11).

We calculated visibility using the NOAA/Forecast Systems Laboratory (FSL) formula developed by Doran et al. (1999) by considering its simplicity. The formula (Eq. 1) uses air temperature, dew point temperature, and relative humidity, essentially the variables we used to assess the model performance.

$$Vis(km) = 1.609 \times 6000 \times [(T - Td)/RH^{1.75}] \qquad (1)$$

Visibility for the PBL and radiation sensitivity simulations is calculated based on the formula in Eq. 1. All PBL schemes develop fog much earlier than the observations at Ataturk Airport, most likely because they simulate a moister boundary layer than the observed one (Fig. 12a). However, differing largely from the others, the YSU-SW1-LW1 simulated the onset of the morning fog only 2 h earlier. Dissipation of the morning fog was simulated much earlier than the observation for all simulations except the YSU (with RRTMG-fast short and RRTMG long-wave radiation schemes) and the YSU-SW1-LW1, all of which produced dissipation only about 2 h before the observation (Fig. 12a). The estimated visibility during the non-fog hours (around noon) was higher than the observations for almost all simulations. The visibility generated by the YSU-SW1-LW1 was somewhat lower than the others. Nearly all local PBL schemes and YSU-SW24-LW1 non-local schemes were able to simulate the evening fog late at Ataturk Airport. The YSU, YSU-SW1-LW1, and BouLac simulations reproduced the onset of the evening fog about the same time as the observation.

Figure 12b depicts the visibility for Sabiha Gokcen Airport. The low visibility conditions (below 1 km) start the previous day at Sabiha Gokcen Airport, and lasts until about
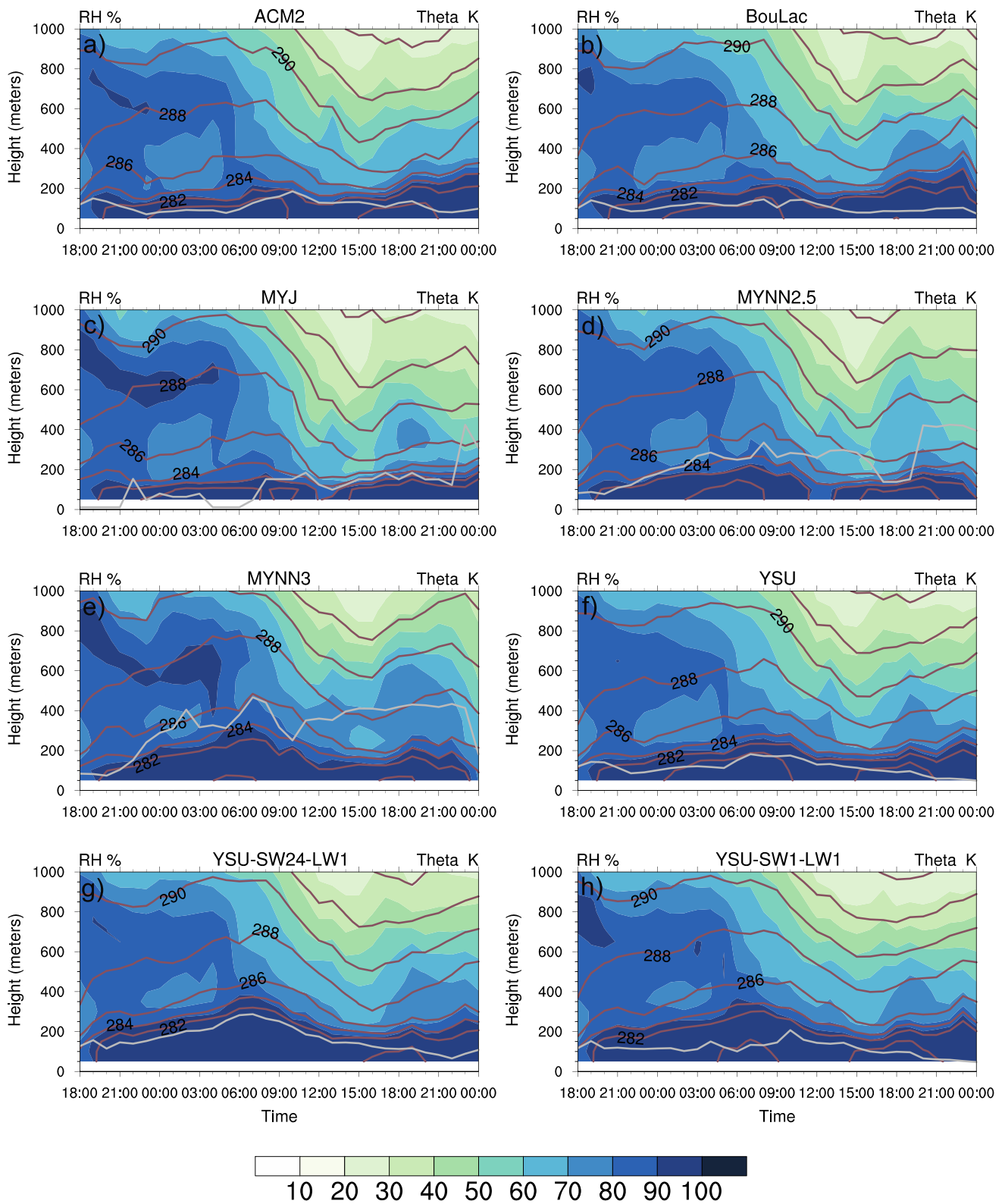
Fig. 8 Time-height changes of relative humidity (shaded) and potential temperature (solid red lines) and simulated PBL height (gray solid line) at Ataturk Airport. **a** ACM2, **b** BouLac, **c** MYJ, **d** MYNN2.5, **e** MYNN3, **f** YSU, **g** YSU-SW24-LW1, and **h** YSU-SW1-LW1
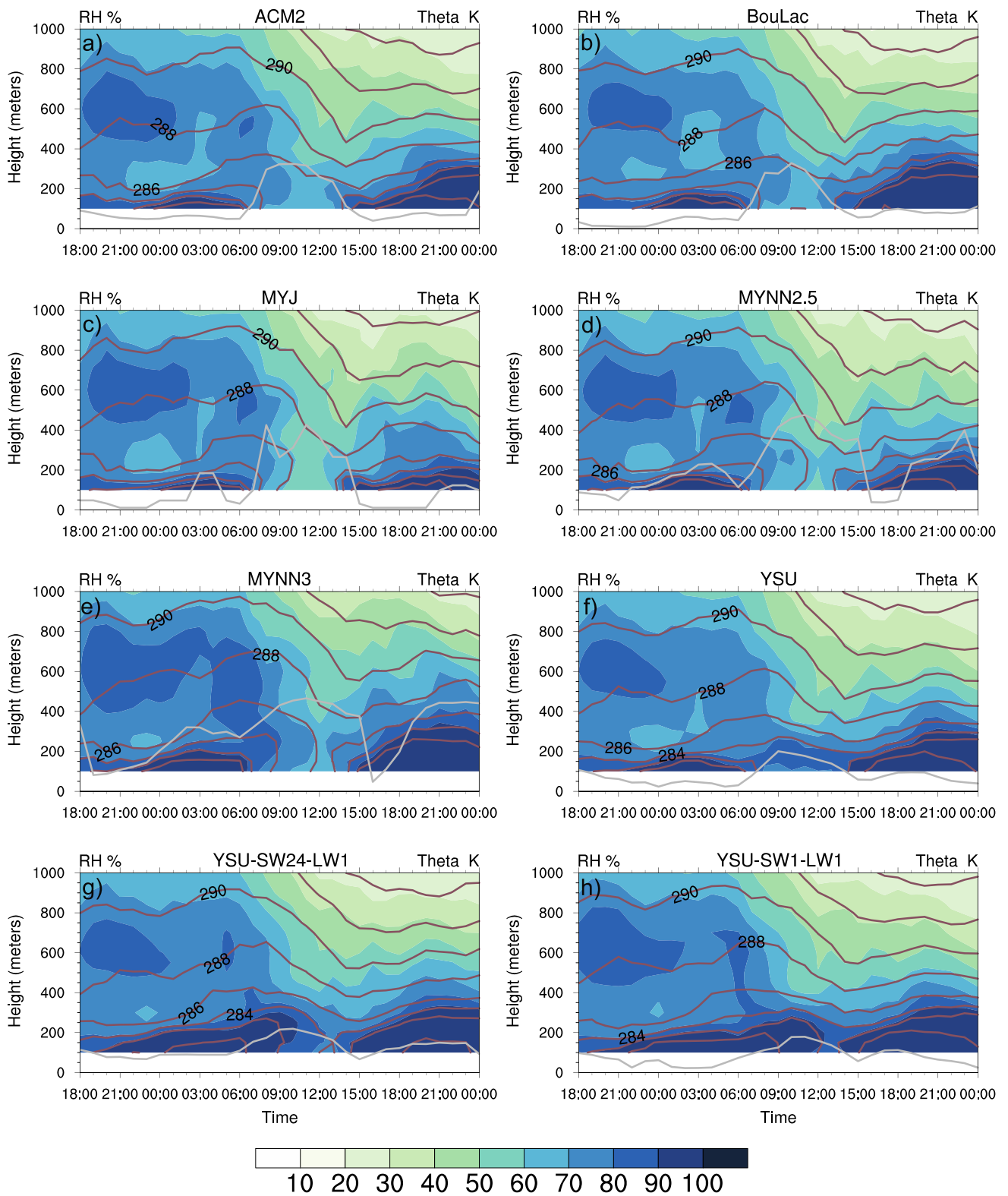
Fig. 9 Time-height changes of relative humidity (shaded) and potential temperature (solid red lines) and simulated PBL height (gray solid line) at Sabiha Gokcen Airport. **a** ACM2, **b** BouLac, **c** MYJ, **d** MYNN2.5, **e** MYNN3, **f** YSU, **g** YSU-SW24-LW1, and **h** YSU-SW1-LW1
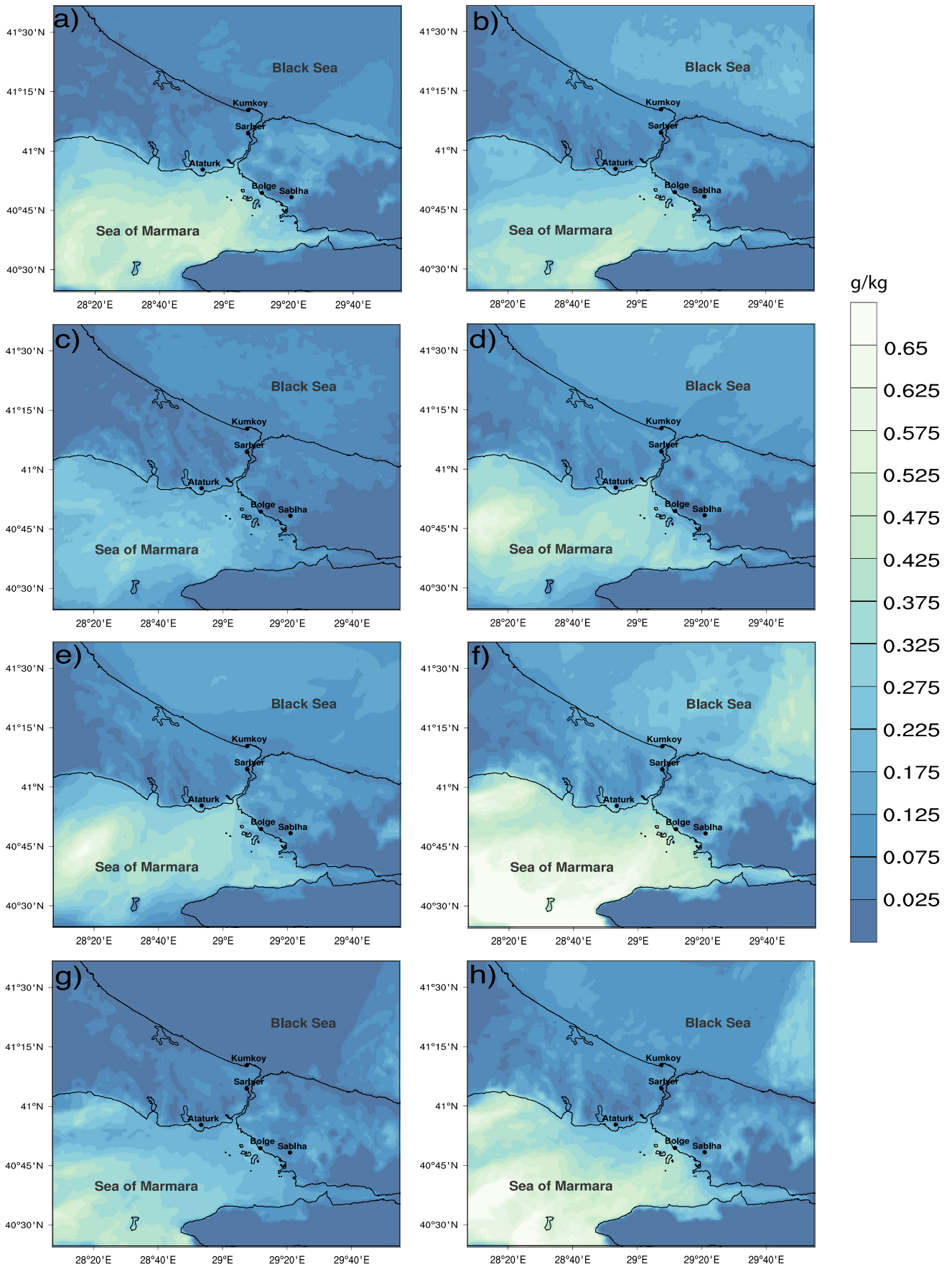
◀**Fig. 10** First model level daily liquid water content (LWC; g/kg) of sensitivity simulations over the innermost domain. **a** ACM2, **b** Bou-Lac, **c** MYJ, **d** MYNN2.5, **e** MYNN3, **f** YSU, **g** YSU-SW24-LW1, and **h** YSU-SW1-LW1

0700 UTC in the morning when the conditions become normal. The visibility decreases below the threshold (1 km) around 1500 UTC in the afternoon and remains low until midnight. It is possible to say that the performance of PBL schemes at Sabiha Gokcen were better than that at Ataturk Airport. However, nearly all simulations reproduced the morning fog later than the observation. Still, the YSU and YSU-SW24-LW1 simulations did a better job by producing the morning fog earlier than the others. The simulation with MYJ produced the shortest duration for the morning fog. The morning fog was dissipated an hour earlier than the observation by all simulations except the YSU-SW1-LW1, which dissipated it one hour later than the observation. As in Ataturk Airport, the evening fog was well reproduced by all simulations. The onset time of the fog was still given with an hour delay by all simulations except the YSU-SW1-LW1 that started the fog the exact same time as the observation (Fig. 12b).

### 3.2 Assessment of sensitivity to non-physics options

In addition to physics parameterizations, we conducted a few sensitivity simulations to test the WRF configuration response to initial and boundary conditions data. The sensitivity experiment on physics parameterizations produced a comparatively good agreement between the observations and the YSU-SW1-LW1 configuration, which included the combination of the YSU PBL scheme with the Milbrandt MP scheme, Dudhia short-wave, and RRTM long-wave schemes. In this part of the study, using the same configuration we forced the model with two different initial and boundary conditions datasets, which are FNL (NCEP Global Prediction System final analysis) with $1 \times 1°$ horizontal resolution and ECMWF ERA5 with $0.30 \times 0.30°$ horizontal resolution. Furthermore, we also examined the role of SST in the fog prediction by forcing the YSU-SW1-LW1 with ERA-Interim data with $0.25 \times 0.25°$ OISST dataset (ERAINT-OISST) since the stability and turbulence near the surface (below 100 m) are sensitive to SST (Gao et al. 2007).

Figure 13 demonstrates that the use of the coarsest dataset, FNL, leads to the poorest results for the fog lifecycle simulation. Visibility calculated based on the variables from this simulation shows that the morning fog does not exist, and the afternoon fog period is very short at Ataturk (Fig. 13g). Meanwhile, the simulation produced a comparatively short (about 2 h) morning fog and an afternoon fog whose onset was delayed for about one hour at Sabiha

Gokcen (Fig. 13h). The use of ERAINT and ERA5 datasets resulted in some differences in simulating the lifecycles of the fog events. Dew point temperature and RH had similar diurnal variations to observations for two airports, however, temperature depression was slightly overestimated by ERA5 at Ataturk during the nighttime and before noon (Fig. 13a). It was also overestimated before the noon at Sabiha Gokcen (Fig. 13b). ERA5 and ERAINT cases produced similar RH variations during the simulation period, and they both broadly captured the observed variations at both airports except for noontime at Sabiha Gokcen when both overestimated it (Figs. 13c and d). Figures 13e and f indicate that the lowest model level had a smaller amount of cloud liquid water in the ERA5 simulation than both ERAINT and FNL simulations at both airports. The estimated visibility at Ataturk Airport showed that the start time of the morning fog is well simulated by the ERA5 case, but the fog was dispersed 2 h earlier compared to the observation.

It should be noted that the ERAINT case simulated the duration of morning fog correctly, but 2 h ahead of the observation at Ataturk Airport (Fig. 13g). The ERA5 case simulated a shorter fog period than the observation. Figure 13g indicates that the ERA5 case starts afternoon fog later than both ERAINT and observation, and ends it after 2200 UTC although the fog continues until the early hours of the following day. For the lifecycle of the fog at Sabiha Gokcen (Fig. 13h), the ERA5 case estimated the start of the morning fog earlier, but it switched back and forth between fog and mist until 0500 UTC when it simulated the final hours of the morning fog which disappeared at the same time as the observation. The ERA5 simulated the afternoon fog fairly well. The overall assessment showed that the performances of the ERAINT and ERA5 cases in terms of the fog simulation were close to each other, but the ERAINT data can be preferred because the simulation-driven with it gives slightly better results than the simulation with the ERA5 data. RMSE values for temperature depression, RH, and wsp for fog hours at Sabiha Gokcen Airport under ERA5 forcing data were 0.23 °C and 2.2% and 2.7 knots, respectively. They were worse when FNL data were used (0.43 °C, 2.92%, and 1.98 knots, respectively). In addition, the ERA5 case performed better than the FNL case at Ataturk Airport (0.79 vs 1.6 °C, 3.69 vs 2.96%, and 4.97 vs 9.23 knots for dew point temperature, RH, and, wsp, respectively). Statistical scores for the entire simulation period also produced better results for the ERA5 case compared to FNL case at both airports. The ERAINT case, however, yielded slightly better performance than the former.

The non-physics sensitivity experiment also included a simulation investigating the effect of different SST data on fog forecasting. Figures 13b and d depict that the ERAINT-OISST included simulation makes some improvement on temperature depression and RH estimation around noon at
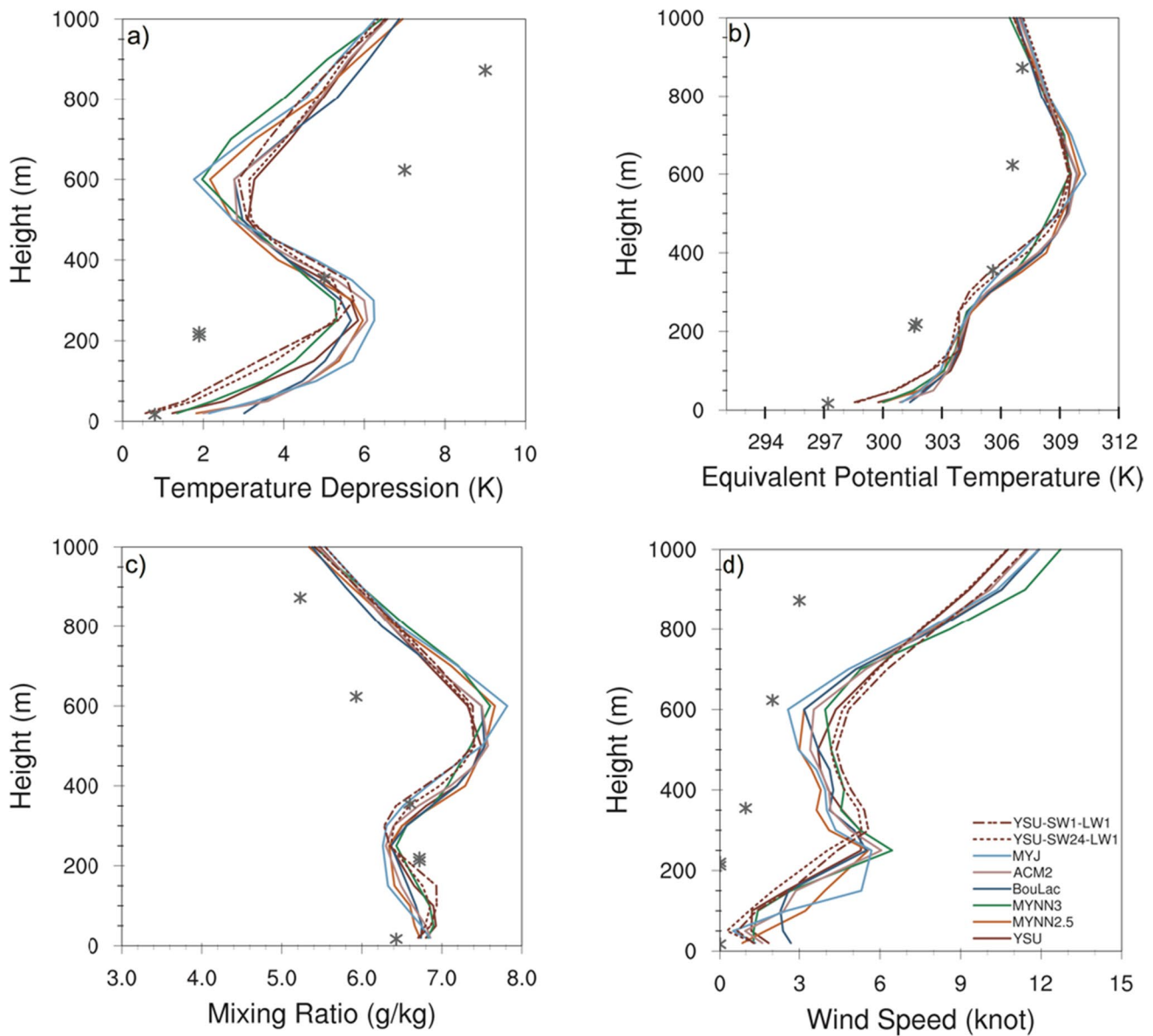
Fig. 11 Observed and modeled vertical variations of **a** temperature depression, **b** equivalent potential temperature, **c** mixing ratio, and **d** wind speed at Bolge station and the corresponding model grid, respectively, on February 19, 2014 0000 UTC. Black asterisks show observed data

Sabiha Gokcen Airport over the ERAINT simulation. However, the performance of the model for these two parameters gets worse around noon at Ataturk Airport (Figs. 13a and c). Both cases simulated these parameters almost similarly during the morning and afternoon fog events. Cloud liquid water content (LWC) is not available in the observations; thus, we can only make comparisons between the simulations, however, it is helpful to improve the prediction of the onset and dissipation times of the fog. At Sabiha Gokcen Airport, the ERAINT-OISST simulation produces lower LWC at the lowest model level during the fog events (Fig. 13f). Ataturk airport yields lower LWC during the morning fog event and higher LWC during the afternoon fog event (Fig. 13e).

The simulated decrease in visibility and the corresponding increase in LWC at Ataturk Airport at around 0600 UTC (Figs. 13e and g) shows that the ERAINT-OISST simulation predicts the onset time of the morning fog well. Figure 13h indicates that the morning fog onset simulated by the ERAINT-OISST case is close to the observation at Sabiha Gokcen. The dissipation of the morning fog starts earlier (later) than the observation at Ataturk (Sabiha Gokcen) Airport for both simulations. However, the early fog dissipation in the ERAINT-OISST case improves the fog lifecycle simulation in the morning at Sabiha Gokcen (Figs. 13h). It is opposite at Ataturk Airport, where LWC decreased immediately after 0700 UTC (Figs. 13e and g). Both ERAINT
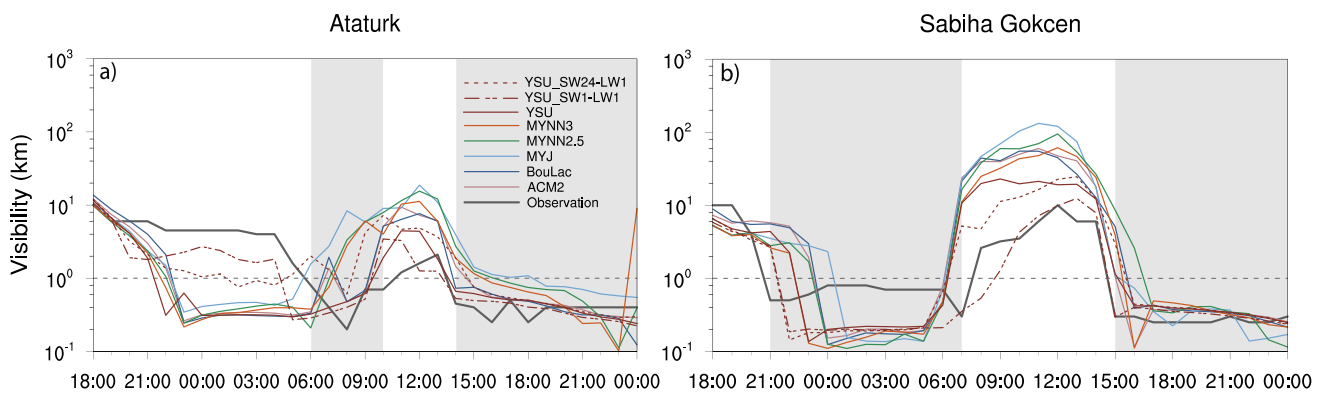
Fig. 12 Diurnal visibility variation from sensitivity simulations and observations for **a** Ataturk and **b** Sabiha Gokcen airports. Gray shades and the horizontal solid line indicate the fog hours from METAR data and visibility threshold for the fog existence, respectively

simulations reproduce the afternoon fog at the same time (1500 UTC) as the observation at Sabiha Gokcen Airport (Figs. 13h). But, the ERAINT-OISST case starts about 1 h later than the observation and ERAINT simulation at Ataturk Airport (Fig. 13g). Statistical evaluation of these two simulations indicates that forcing the model with observed SST data does not significantly improve fog simulation at either airport. RMSE values of temperature depression, RH, and wsp were 0.4 °C (0.31 °C), 2.5% (2.79%), and 3.09 knot (1.8 knot) at Ataturk (Sabiha Gokcen) airport, respectively.

### 3.3 Comparison of YSU-SW1-LW1 simulation with satellite observations

The sensitivity simulations, including physics and non-physics processes, suggest that the model configuration comprising the YSU PBL, Milbrandt scheme with Tiedtke cumulus parameterization shows fairly good performance in simulating the fog events. The sensitivity simulations on radiation schemes indicate that the YSU-SW1-LW1 case provides better results than the others investigated in this study. To gain more insight into the model performance, we qualitatively compared the YSU-SW1-LW1 simulation outputs with the MODIS Terra and Aqua acquired data. MODIS observations provide two relevant products (cloud reflectance and cloud water path) on the day of the fog that was studied. These products are available at 11:55 a.m. from MODIS Aqua and at 08:35 a.m. from MODIS Terra. Figure 14a shows the morning fog/low cloud coverage over Istanbul and its vicinity. The morning fog/low clouds are relatively dense along with the coastal parts of the city. Both the south and north coasts and the strait are under the influence of the fog. Also, in line with the ground observations both airports seem to be affected by the fog event. Figure 14d indicates that the fog retracts

toward water surfaces, especially in the south around noon. This cloud was recorded as mist in the ground observations. The dense fog dissipates over the province of Istanbul largely by noon.

Wærsted et al. (2017) state that CWP is greater than 30 gm^{-2} in an opaque fog. CWP from the MODIS TERRA data (Fig. 14b) indicates thick clouds in the western parts of the city in the morning. CWP from the MODIS Aqua (Fig. 14e) shows relatively thin clouds in the western part at around noon while thicker clouds in the eastern part with greater CWP than 200 gm^{-2}. In order to compare model estimations with satellite observations, we calculated the liquid water path (LWP), a measure of the total amount of liquid water in the atmospheric column, from the YSU-SW1-LW1 simulation. LWP (gm^{-2}) is calculated between the surface (Psfc; lowest model level) and top of the atmosphere (Ptop; 50 hPa) based on liquid water mixing ratio (r; g/kg) and gravitational acceleration (g; ms^{-2}), as follows (Eq. 2).

$$\mathrm{LWP} = \int_{\mathrm{Psfc}}^{\mathrm{Ptop}} \mathrm{rdP}/g \tag{2}$$

Although CWP includes both LWP and ice water path (IWP), the WRF model does not produce an ice mixing ratio at the times of MODIS observations (not shown), therefore we compared modeled LWP with observed CWP qualitatively. Figures 14c and f present the calculated LWP over Istanbul for the times of the MODIS observations. The comparison indicates that the modeled LWP distribution matches with the visible images more (Figs. 14a and d). LWP is greater than 20 gm^{-2}, mostly over the water surfaces. Similar to the MODIS CWP in Fig. 14b, LWP is over 30 gm^{-2} in the west of the domain at noon. However, LWP of values greater than 20 gm^{-2} is seen over the water
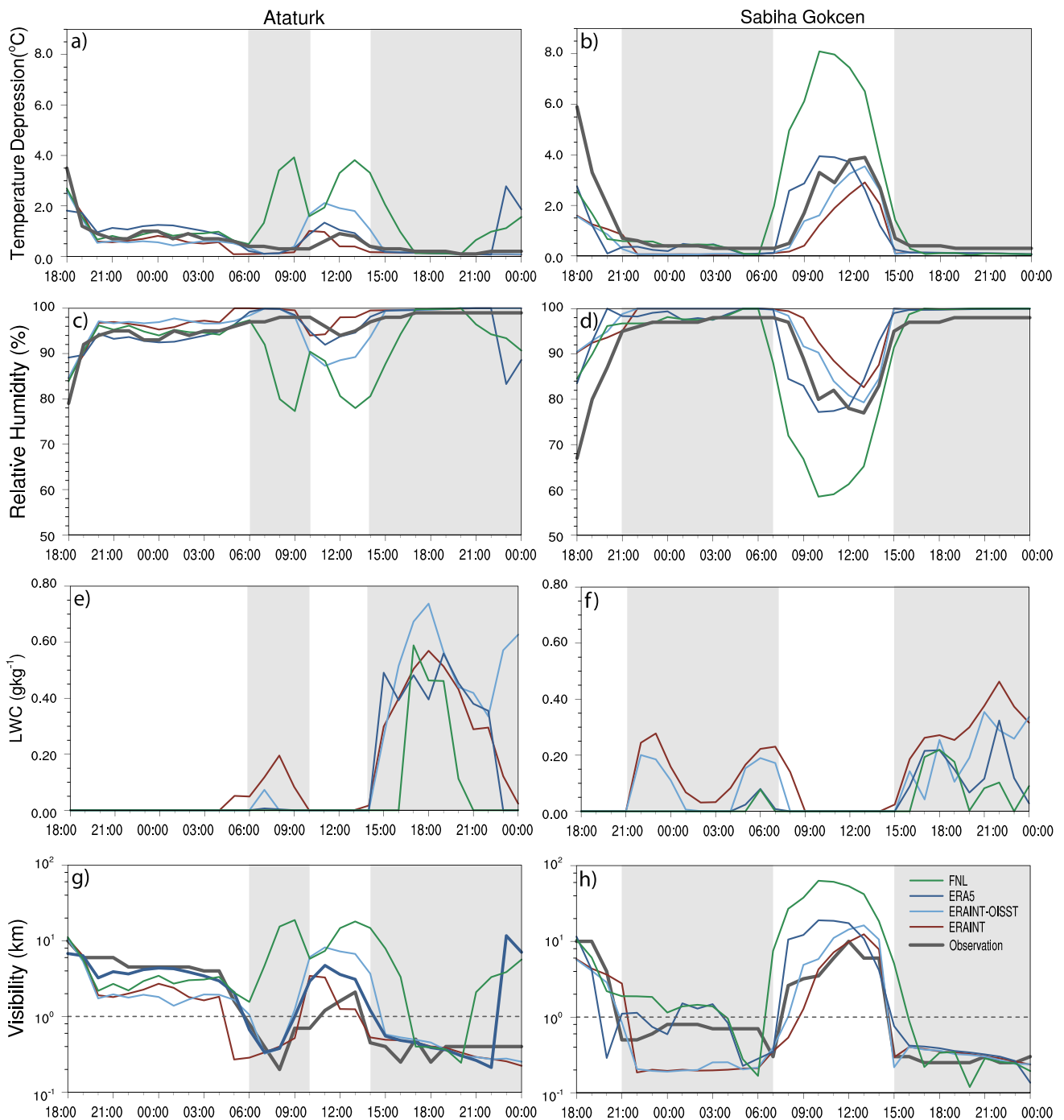
Fig. 13 Results of initial and boundary condition sensitivity simulations. Temperature depression (**a** and **b**), RH (**c** and **d**), LCW (**e** and **f**), and visibility (**g** and **h**) for Ataturk (left) and Sabiha Gokcen (right) airports. Gray shading and gray dash line point out the foggy hours from METAR data and visibility threshold for the fog existence, respectively

body in the south of Istanbul, penetrating only the coastal areas. It looks quite different from the CWP obtained from MODIS Aqua.

4 Summary and discussion

Fog, which is an important meteorological phenomenon adversely affecting land, air, and sea transportation, is difficult to predict. This paper aims to assess the performance of the WRF model in simulating a dense advection fog event in
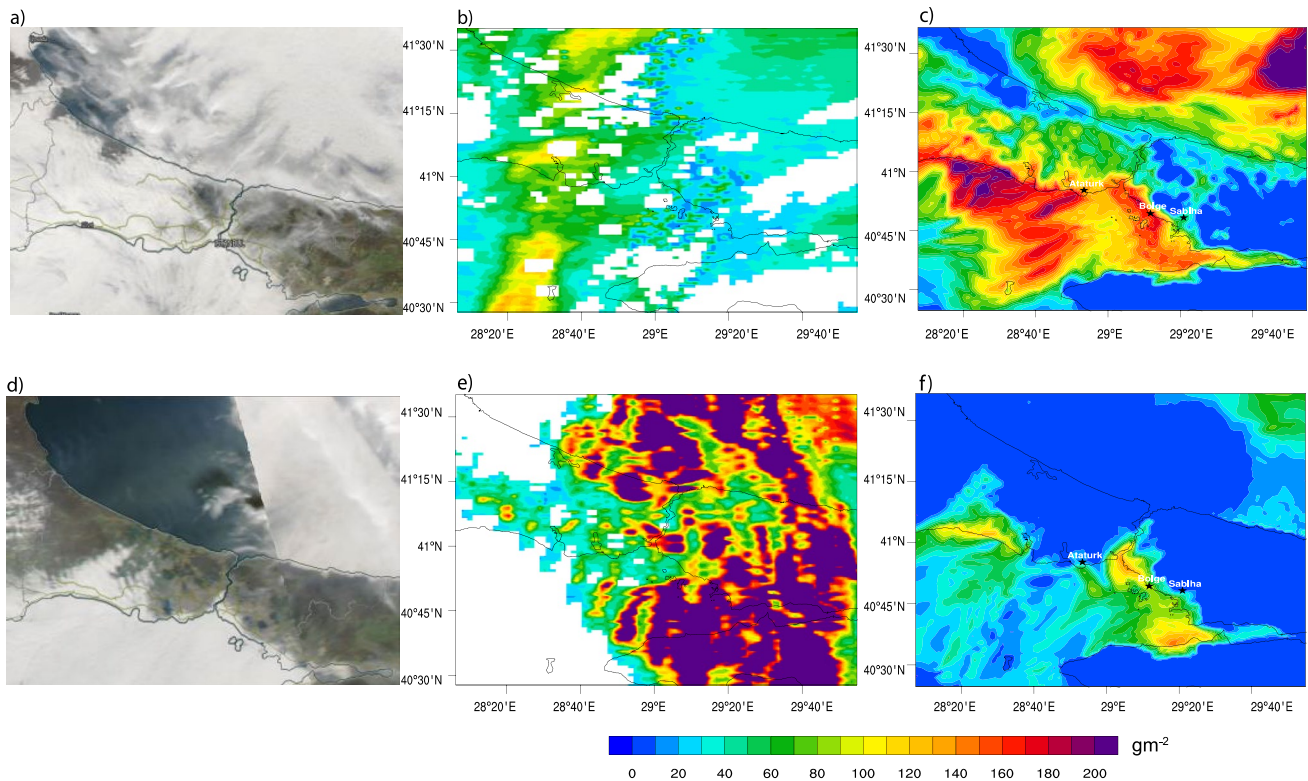
Fig. 14 Corrected reflectance and cloud water path (CWP, gm^{-2}) from MODIS Terra (**a** and **b**) at 08:35 am and Aqua (**d** and **e**) at 11:55 a.m., respectively, and liquid water ath (gm^{-2}) calculated from the model (**c** and **f**) at the times associated with Terra and Aqua data, respectively

Istanbul through sensitivity simulations involving different physics options and initial and boundary condition data sets. The fog event chosen for the sensitivity experiment occurred on February 19, 2014 with suitable synoptic conditions.

Previous studies showed that fog dissipation is highly sensitive to microphysics schemes (e.g., Lin et al. 2017 and Steeneveld et al. 2015). Therefore, we first tested the model by performing sensitivity simulations on the available six microphysics schemes with the MYNN2.5 PBL scheme. All these simulations produced warm temperature bias between 0600 and 1500 UTC. This caused a rapid dissipation of the fog during this period. The simulations with all microphysics schemes produced a moist atmosphere early in the morning and late at night, and a dry atmosphere during the daytime. Wind speed was also important for the fog dissipation, and all these simulations reproduced the diurnal variations of wind speed at two airports fairly well. The model was generally better in simulating temperature at Ataturk Airport than at Sabiha Gokcen Airport. The simulation with the Milbrandt scheme had relatively low MB (0.71 and 1.25 °C for Ataturk and Sabiha Gokcen airports, respectively) and RMSE (1.18 and 2.5 °C for Ataturk and Sabiha Gokcen airports, respectively) of temperature. Also, relatively low MB (0.56 and 0.13 °C for Ataturk and Sabiha Gokcen airports, respectively) and

RMSE (1.15 and 0.89 °C for Ataturk and Sabiha Gokcen, respectively) values suggested that the dew point temperature variations were quite well captured by WRF with this scheme at both airports. Results revealed that the use of different cumulus parameterizations did not produce changes in the fog simulation.

After setting Milbrandt as the microphysics scheme, Tiedtke as the cumulus scheme, and RRTMG as the radiation (both short and longwave radiation) scheme, we tested different PBL schemes through further sensitivity simulations. The simulations depicted a typical daytime warm (cold) bias in temperature (dew point temperature). The performance of each PBL scheme was quite good for Sabiha Gokcen Airport however, it was not that good for Ataturk Airport, which is closer to a water body. These sensitivity simulations revealed that PBL schemes did not have much control on the onset and the dissipation of the fog. Our result supports Lin et al. (2017), who stated that the timing of formation and dissipation of fog was sensitive to longwave and shortwave radiation schemes. The simulations with PBL schemes together with RRTMG-fast shortwave and RRTMG longwave radiation schemes resulted in decreases in daytime temperature bias. Especially the decrease achieved by the simulation, including the YSU PBL scheme with these radiation schemes was noteworthy.

Studies such as Roman-Cascon et al. (2012), Chaouch et al. (2017), and Pithani et al. (2019a and 2019b) concluded that local PBL schemes provided better results than the non-local ones. However, in contrast with their findings, our results revealed that the non-local PBL scheme YSU performed relatively better than local schemes. A similar result was also presented by Steeneveld et al. (2015) and Lin et al. (2017). Both local and non-local PBL schemes involve representation of the vertical mixing processes. In general, the non-local YSU schemes (with first-order closure parabolic K-profile) with the entrainment flux proportional to the surface flux are favorable in unstable conditions while local PBL schemes (with TKE closure) show better performance in stable conditions (Shin and Hong 2011). Nonetheless, the modified YSU formulation with an increase in the critical bulk Richardson number from zero to 0.25 (Hong et al. 2006) enhances the representativeness of the mixing in a stable layer (Hu et al. 2010). It is known that the lowest part of the planetary boundary layer is directly affected by surface exchanges of heat, momentum, and moisture (Stull 1988). In the WRF model, the surface layer schemes corresponding to the PBL schemes define the surface exchange coefficients to calculate sensible heat, latent heat, and momentum fluxes. Further analysis revealed that the fog event distinctions between the PBL schemes could partly be related to the differences in the heat fluxes, especially in the sensible heat flux, at the surface (see Figure S5). Therefore, the surface cooling is mixed in a shallower layer in YSU than the local schemes and also in ACM2, which uses a hybrid closure scheme (a first-order, non-local closure scheme that represents non-local upward mixing and local downward mixing). Our results showed that YSU-SW1-LW1 differs from the other PBL schemes with its lower sensible heat fluxes. Avolio et al. (2017) suggest that sensible heat flux plays an important role in the performance of WRF at the local scale. It was found by Kim and Yum (2017) that longwave radiation was more important in the net radiation budget for the formation and development of marine fog. It is noted that YSU was more sensitive to radiation schemes, therefore RRTM (RRTMG-fast) longwave (shortwave) and Dudhia (RRTM) shortwave (longwave) schemes were run together with the YSU PBL. Overall, simulations with different PBL schemes well-simulated the temperature depression under the fog influence at both airports. However, error statistics were evidently better at Ataturk Airport. The simulation with the YSU scheme came out with lower RMSE values than the others. The effects of short and long-wave radiations on fog prediction differed for two stations. Namely, the simulations with RRTMG-fast and RRTMG performed better at Ataturk in terms of temperature depression and RH. However, it was the combination of Dudhia and RRTM schemes that gave better results at Sabiha Gokce. The model had moister conditions than the observations from the surface up to 300 m in

the atmosphere for all sensitivities. The model had stronger winds for the lowest 1 km of the atmosphere than the observations from the sounding measurements. The YSU-SW1-LW1 simulation reproduced both the onset and dissipation times of the morning fog 2 h earlier than the observations at Ataturk and an hour later than the observations at Sabiha Gokcen. The onset time of the afternoon fog was well captured by the YSU-SW1-LW1 simulation.

The pattern of the simulated LWP from the YSU-SW-LW1 simulation matched well with the cloud products from MODIS Terra and Aqua observations. These observations depicted high liquid water content over the water bodies especially in the morning when the MODIS Terra image was available. MODIS Aqua image also provided that LWC was relatively high in the south of the city at noon.

In an attempt to further understand how the configurations with PBL and radiation schemes represent the fog life cycle during the advection fog events, we carried out simulations for two more fog events in Istanbul. The events took place on December 15, 2014 (see Supplementary Figures S6–S15) and March 1, 2017 (see supplementary figures S16–S25). Similar to the February 19, 2014 fog event, synoptic pattern in the latter has southwesterly moist air inclusion from the south of the province of Istanbul, however the December 15, 2014 case has a southeasterly flow prevailing over the region with a more pronounced cold air blowing from the northeast. The model results are comparable to the fog event investigated in the present study (the February 19, 2014 case). The sensitivity simulations for these three fog events demonstrate that the model with the non-local YSU-PBL scheme and Dudhia shortwave and RRTM longwave radiation schemes is able to reproduce fog events fairly well, but with deviations in the onset and dissipation times.

For the February 19, 2014 case, we further analyzed the effects of the different forcing datasets on the formation, duration, and dissipation of the fog using IC-BCs provided by ECMWF and NCEP. We tested mainly three different forcing datasets, ERA-Interim, ERA5, and FNL, to simulate the event. FNL results were found to be comparatively poor. Forcing the model with the high-resolution ERA5 data depicted an improvement in the timing of the morning fog onset at Ataturk, however, it dissipated the fog earlier than the observation. The use of ERA5 also delayed the formation of the afternoon fog. Furthermore, the morning fog was formed earlier, and its dissipation time was slightly earlier than the observations at Sabiha Gokcen. Both ERA5 and ERA-Interim forcing produced the onset time of the afternoon fog at the same time as the observation. It was found that using a relatively higher-resolution sea surface temperature dataset did not improve the performance of the simulations, especially at Ataturk, a coastal airport.

There are other important factors that could affect the predictability of a fog event, but they are not investigated in

this study. For instance, Lin et al (2017) stated that an appropriate forecast lead time is important for the spin-up of the model and completion of the physical processes. Moreover, urbanization and aerosols have an impact on fog forecasting. Heavy air pollution reduces the longwave radiation cooling, and hence affect the formation of the fog (Li et al. 2019). Also, urbanization speed affects the formation of fog. Fog formation is supported by the abundance of aerosols during the slow urbanization while it is inhibited during the rapid urbanization due to the urban heat island effect (Yan et al. 2019). Urban expansion influences all types of fog formation (Gu et al. 2019). Since Istanbul is a densely populated megacity and the border of the urban region expands northward, there is an urgent need to further investigate the impact of urbanization on the fog formation over the city.

5 Conclusion

The aim of this study is to investigate the performance of WRF (version 3.9.1.1) in simulating a dense advection fog in Istanbul, which especially affects national and international air traffics and local transportation adversely. The sensitivity experiment involved hierarchical simulations with different microphysics, PBL, radiation parameterizations, and different forcing datasets. The conclusions are as follows:

- Milbrandt microphysics scheme performs slightly better than the other schemes used in the study.
- Non-local PBL schemes are better at simulating the diurnal cycle than the others. Although the statistics suggest that all the PBL schemes give good simulations at the fog hours, it is the YSU PBL scheme that gives better timings for the formation and dissipation of the fog.
- The model produces a warm temperature bias during the daytime. Different configurations with longwave and shortwave radiation schemes reveal that longwave and shortwave radiation parameterization is more effective than the others in eliminating the bias.
- The YSU PBL scheme with RRTM longwave and Dudhia shortwave radiation schemes (the YSU-SW1-LW1 simulation) perform comparatively well for the simulation of the advection fog. Although this configuration gives comparatively better results compared to the other configurations, our study indicates that each fog events have different features. Therefore, we cannot generalize that the performance of this model configuration changes from one case to another, since fog events have different features. The synoptic-scale conditions of each event are case-specific, and also the interaction of mesoscale features with the synoptic scale features differs over different regions.

- The simulated wind speed is comparatively weak along the coast for the morning fog, therefore the development of the fog, hence the onset and dissipations, occurs early along the coast. The model simulates the onset time of the afternoon fog pretty well.
- High-resolution IC-BC data do not provide a significant improvement in fog simulation. Results show that ERA-Interim performs slightly better than the ERA5 dataset.

There is a need to investigate the effect of spin-up time on the simulation of the wind field, which may have an important role in the advection of the fog along the coast. Thus, we are planning to investigate the effects of spin-up time, pollutant particles, and urbanization with model parameterizations in our future studies. We will also attempt to analyze more cases of advection and radiation fog types.

Author contribution Yasemin Ezber: formal analysis, visualization, methodology, investigation, writing original draft, and editing. Omer Lutfi Sen: conceptualization, investigation, and writing—review and editing.

Data availability The datasets generated during the current study are available from the corresponding author on reasonable request.

Code availability The datasets analyzed during the current study are available from the corresponding author on reasonable request.

Declarations

Ethics approval The authors have no relevant financial or non-financial interests to disclose.

Consent for publication All persons who meet authorship criteria are listed as authors, and all authors certify that they have participated sufficiently in the work to take public responsibility for the content, including participation in the concept, design, analysis, writing, or revision of the manuscript. Furthermore, each author certifies that this material or similar material has not been and will not be submitted to or published in any other publication.

Conflict of interest The authors declare no competing interests.

References

Avolio E, Federico S, Miglietta MM, Lo FT, Calidonna CR, Sempreviva AM (2017) Sensitivity analysis of WRF model PBL schemes in simulating boundary-layer variables in southern Italy: an experimental campaign. Atmos Res 192:58–71

Bari D, Bergot T, El Khlifi M (2015) Numerical study of a coastal fog event over Casablanca. Morocco q J r Meteorol Soc 141:1894–1905. https://doi.org/10.1002/qj.2494

Bendix J, Thies B, Nauss T, Cermak J (2006) A feasibility study of daytime fog and low stratus detection with TERRA/AQUA-MODIS over land. Meteorol Appl 13:111–125

Bergot T, Terradellas E, Cuxart J, Mira A, Liechti O, Mueller M, Nielsen NW (2007) Intercomparison of single-column numerical models for the prediction of radiation fog. J Appl Meteorol Climatol 46:504–521

Bougeault P, Lacarrere P (1989) Parameterization of orography-induced turbulence in a Mesobeta–scale model. Mon Weather Rev 117:1872–1890

Byers HR (1959) General Meteorology. McGraw-Hill, New York

Cermak J, Eastman RM, Bendix J, Warren SG (2009) European climatology of fog and low stratus based on geostationary satellite observations. Q J R Meteorol Soc 135:2125–2130

Chaouch N, Temimi M, Weston M, Ghedira H (2017) Sensitivity of the meteorological model WRF-ARW to planetary boundary layer schemes during fog conditions in a coastal arid region. Atmos Res 187:106–127

Dee DP, Uppala SM, Simmons AJ, Berrisford P, Poli P, Kobayashi S, Andrae U, Balmaseda MA, Balsamo G, Bauer P, Bechtold P, Beljaars ACM, van de Berg L, Bidlot J, Bormann N, Delsol C, Dragani R, Fuentes M, Geer AJ, Haimberger L, Healy SB, Hersbach H, Holm EV, Isaksen L, Kallberg P, Koehler M, Matricardi M, McNally AP, Monge-Sanz BM, Morcrette JJ, Park BK, Peubey C, de Rosnay P, Tavolato C, Thepaut JN, Vitart F (2011) The ERA-Interim reanalysis: configurationand performance of the data assimilation system. Q J r Meteorolog Soc 137:553–597

Doran JA, Roohr PJ, Beberwyk DJ, Brooks GR, Gayno GA, Williams RT, Lewis JM, Lefevre RJ (1999) The MM5 at the air force weather agency—new products to support military operations. In: Proceedings of the 8th conference on aviation, range, and aerospace meteorology, NOAA/NWS, Dallas, Texas

Dudhia J (1989) Numerical study of convection observed during the Winter Monsoon Experiment using a mesoscale two–dimensional model. J Atmos Sci 46:3077–3107

Dupont J-C, Haeffelin M, Protat A, Bounil D, Boyouk N, Morille Y (2012) Stratus-fog formation and dissipation: a 6-day case study. Bound-Layer Meteorol 143:207–225

Ellord GP, Gultepe I (2007) Inferring low cloud base heights at night for aviation using satellite infrared and surface temperature data. Pure Appl Geophys 164:1193–1205

Ellrod GP (2002) Estimation of low cloud base height at night from satellite infrared and surface temperature data. Natl Wea Dig 26:39–44

Eyre JR, Brownscombe JL, Allan RJ (1984) Detection of fog at night using advanced very high resolution radiometer (AVHRR) imagery. Meteorol Mag 113:66–271

Gao S-H, Lin H, Shen B, Fu G (2007) A heavy sea fog event over the Yellow Sea in March 2005: analysis and numerical modeling. Adv Atmos Sci 24(1):65–81

Gu Y, Kusaka H, Doan VQ, Tan J (2019) Impacts of urban expansion on fog types in Shanghai, China: numerical experiments by WRF model Ying. Atmos Res 220:57–74

Guls I, Bendix J (1996) Fog detection and fog mapping using low cost Meteosat WEFAX transmission. Meteor Appl 3:179–187

Gultepe I, Tardif R, Michaelides S, Cermak J, Bott A, Bendix J, Muller MD, Pagowski M, Hansen B, Ellrod G, Jacobs W, Toth G, Cober SG (2007) Fog research: a review of past achievements and future perspectives. Pure Appl Geophys 164:1121–1159

Gultepe I, Pearson G, Milbrandt JA, Hansen B, Platnick S, Taylor P, Gordon M, Oakley JP, Cober SG (2009) The fog remote sensing and modeling (FRAM) field project. Bull Amer Meteor Soc 90:341–359

Gultepe I, Zhou B, Milbrandt J, Bott A, Li Y, Heymsfield AJ, Ferrier B, Ware R, Pavolonis M, Kuhn T, Gurka J, Liu P, Cermak J (2015) A review on ice fog measurements and modeling. Atmos Res 151:2–19

Haeffelin M, Bergot T, Elias T, Tardif R, Carrer D, Chazette P, Colomb M, Drobinski P, Dupont J-C, Gomes L, Musson-Genon L, Pietras C, Plana-Fattori A, Protat A, Rangognio J, Raut J-C, Rémy S, Richard D, Sciare J, Zhang X (2010) Parisfog: shedding new light on fog physical processes. Bull Amer Meteor Soc 91:767–783

Hahmann AN, Sile T, Witha B, Davis NN, Dörenkämper M, Ezber Y, García-Bustamante E, Fidel González Rouco J, Navarro J, Olsen BT, Söderberg S (2020) The making of the New European Wind Atlas – part 1: model sensitivity. Geosci Model Dev 13:5053–5078. https://doi.org/10.5194/gmd-13-5053-2020

Herzegh P, Wiener G, Bankert R, Benjamin S, Bateman R, Cowie J, Hadjimichael M, Tryhane M, and Weekley B (2006) Development of FAA national ceiling and visibility products: challenges, strategies and progress, Perprints 12th Conference on Aviation Range and Aerospace Meteorology. Am Meteor Soc, Atlanta, GA

Hong SY, Lim JOJ (2006) The WRF single-moment 6-class microphysics scheme (WSM6). J Korean Meteorol Soc 42:129–151

Hong S-Y, Noh Y, Dudhia J (2006) A new vertical diffusion package with an explicit treatment of entrainment processes. Mon Weather Rev 134:2318–2341

Hu X-M, Nielsen-Gammon JW, Zhang F (2010) Evaluation of three planetary boundary layer schemes in the WRF model. J Appl Meteor Climatol 49:1831–1844. https://doi.org/10.1175/2010JAMC2432.1

Hu HQ, Zhang QH, Xie BG et al (2014) Predictability of an advection fog event over North China. Part I: sensitivity to initial condition differences. Mon Weather Rev 142:1803–1822

Hutchison KD, Pekker T, Smith S (2006) Improved retrievals of cloud boundaries from MODIS for use in air quality modeling. Atmos Environ 40:5798–5806

Iacono MJ, Delamere JS, Mlawer EJ, Shephard MW, Clough SA, Collins WD (2008) Radiative forcing by long-lived greenhouse gases: calculations with the AER radiative transfer models. J Geophys Res 113:D13103. https://doi.org/10.1029/2008JD009944PDF

Janjic ZI (1994) The step-mountain Eta coordinate model: further developments of the convection, viscous sublayer, and turbulence closure schemes. Mon Weather Rev 122:927–945

Kain JS (2004) The Kain-Fritsch convective parameterization: an update. J Appl Meteor 43:170–181

Karlsson K-G (1989) Development of an operational cloud classification model. Internat J Remote Sensing 10:687–693

Kim CK, and Yum SS (2017) Marine fog: challenges and advancements in observations, modeling, and forecasting, radiation in marine fog (Chapter 5), Springer Nature, Switzerland

Koracin D, Lewis JM, Thompson WT, Dorman CE, Businger JA (2001) Transition of stratus into fog along the California Coast: observations and modeling. J Atmos Sci 58:1714–1731

Lewis JM, Koračin D, Redmond KT (2004) Sea fog research in the United Kingdom and United States: a historical essay including outlook Bull. Amer Meteor Soc 85(3):395–408

Li Z, Liu D, Yan W, Wang H, Zhu C, Zhu Y, Zu F (2019) Dense fog burst reinforcement over Eastern China: a review. Atmos. Res. 230:104639

Lin C, Zhang Z, Pu Z, Wang Y (2017) Numerical simulations of an advection fog event over Shanghai Pudong International Airport with the WRF model. J Meteorol Res 31:874–889

Liu DY, Yan J, Niu SJ, Li ZH (2011) On the evolution and structure of a radiation fog event in Nanjing. Adv Atmos Sci 28(1):223–237

Maier F, Bendix J, Thies B (2013) Development and application of a method for the objective differentiation of fog life cycle phases. Tellus b: Chemical and Phys Meteorol 65(1):19971

Mansell ER, Ziegler CL, Bruning EC (2010) Simulated electrification of a small thunderstorm with two-moment bulk microphysics. J Atmos Sci 67:171–194

Menut L, Mailler S, Dupont J-C, Haeffelin M, Elias T (2013) Predictability of the meteorological conditions favourable to radiative fog formation during the 2011 ParisFog campaign,. Boundary-layer meteorol 150:277–297

Milbrandt JA, Yau MK (2005) A multimoment bulk microphysics parameterization. Part I: Analysis of the role of the spectral shape parameter. J Atmos Sci 62:3051–3064

Milbrandt JA, Yau MK (2005) A multimoment Bulk microphysics parameterization. part ii: a proposed three-moment closure and scheme description. J Atmos Sci 62(9):3065–3081

Mlawer EJ, Taubman SJ, Brown PD, Iacono MJ, Clough SA (1997) Radiative transfer for inhomogeneous atmospheres: RRTM, a validated correlated-k model for the longwave. J Geophys Res 102:16663–16682

Morrison H, Thompson G, Tatarskii V (2009) Impact of cloud microphysics on the development of trailing stratiform precipitation in a simulated squall line: comparison of one and two-moment schemes. Mon Weather Rev 137:991–1006

Muller MD, Masbou M, Bott A (2010) Three-dimensional fog forecasting in complex terrain. Q J R Meteorol Soc 136:2189–2202

Nakanishi M, Niino H (2004) An improved mellor-yamada level-3 model with condensation physics: its design and verification. Boundary-Layer Meteorol 112:1–31

Nakanishi M, Niino H (2006) An improved Mellor-Yamada level 3 model: its numerical stability and application to a regional prediction of advecting fog. Boundary- Layer Meteorol 119:397–407

Ozdemir ET, Deniz A, Sezen İ, Mentes SS, Yavuz V (2016) Fog analysis at Istanbul Ataturk International Airport. Weather 71(11):279–284

Payra S, Mohan M (2014) Multirule based diagnostic approach for the fog predictions using WRF modeling tool. Adv. Meteor. 2014:456065

Pithani P, Ghude SD, Chennu VN, Kulkarni RG, Steeneveld G-J, Sharm A, Prabhakaran T, Chate DM, Gultepe I, Jenamani RK, Madhavan R (2019) WRF model prediction of a dense fog event occurred during the winter fog experiment (WIFEX). Pure Appl Geophys 176:1827–1846

Pithani P, Ghude SD, Prabhakaran T, Karipot A, Hazra A, Kulkarni R, Chowdhuri S, Resmi EA, Konwar M, Murugavel P, Safai PD, Chate DM, Tiwari Y, Jenamani RK, Rajeevan M (2019) WRF model sensitivity to choice of PBL and microphysics parameterization for an advection fog event at Barkachha, rural site in the Indo-Gangetic basin. India. Theor. Appl. Climatol 136:1099–1113

Pleim JE (2007) A combined local and nonlocal closure model for the atmospheric boundary layer. Part I: model description and testing. J Appl Meteor Climatol 46:1383–1395

Price J, Porson A, Lock A (2015) An observational case study of persistent fog and comparison with an ensemble forecast model. Boundary-Layer Meteorol 155:301–327

Remy S, Bergot T (2009) Assesing the impact of observations on a local numerical fog prediction system. Q J R Meteorol Soc 135:1248–1265

Roach WT (1995) Back to basics: fog: part 2-the formation and dissipation of land fog. Weather 50:7–11

Román-Cascón C, Yagüe C, Sastre M, Maqueda G, Salamanca F, Viana S (2012) Observations and WRF simulations of fog events at the Spanish Northern Plateau. Adv Sci Res 8(1):11–18

Ryznar E (1977) Advection-radiation fog near Lake Michigan. Atmos Environ 11:427–430

Shin HH, Hong S-Y (2011) Intercomparison of planetary boundary-layer parameterizations in the WRF model for a single day from CASES-99. Boundary-Layer Meteor 139:261–281

Skamarock WC, Klemp JB, Dudhia J, Gil DA, Barker DM, Duda MG, Huang X-Y, Wang W, Powers JG (2008) Description of the advanced research WRF, version 3. National Center for Atmospheric Research, Boulder, Colorado

Steeneveld G-J, Bode M (2018) Unravelling the relative roles of physical processes in modelling the life cycle of a warm radiation fog. Q J R Meteorol Soc 144:1539–1554

Steeneveld GJ, Ronda RJ, AAM H (2015) The challenge of forecasting the onset and development of radiation fog using mesoscale atmospheric models. Boundary-Layer Meteorol 154:265–289. https://doi.org/10.1007/s10546-014-9973-8

Stolaki S, Pytharoulis I, Karacostas T (2012) A study of fog characteristics using a coupled WRF-COBEL model over Thessaloniki Airport, Greece. Pure Appl Geophys 169:961–981

Stull RB (1988) An introduction to boundary layer meteorology. Kluwer Academic Publishers, Dordrecht, Boston, London, p 666

Tang YM, Capon R, Forbes R et al (2009) Fog prediction using a very high resolution numerical weather prediction model forced with a single profile. Meteor Appl 16:129–141. https://doi.org/10.1002/met.V.16:2

Tardif R (2007) The impact of vertical resolution in the explicit numerical forecasting of radiation fog: a case study. Pure Appl Geophys 164:1221–1240. https://doi.org/10.1007/s00024-007-0216-5

Tardif R, Rasmussen RM (2007) Event-based climatology and typology of fog in the New York City region. J Appl Meteorol Climatol 46:1141–1168

Thompson G, Eidhammer T (2014) A study of aerosol impacts on clouds and precipitation development in a large winter cyclone. J Atmos Sci 71(10):3636–3658

Tiedtke M (1989) A comprehensive mass flux scheme for cumulus parameterization in large–scale models. Mon Weather Rev 117:1779–1800

Toker E, Ezber Y (2020) Sen OL (2021) Numerical simulation and sensitivity study of a severe hailstorm over Istanbul. Atmos Res 250:105373. https://doi.org/10.1016/j.atmosres.2020.105373

Turner J, Allam R, Maine D (1986) A case study of the detection of fog at night using channels3 and 4 on the advanced very high resolution radiometer (AVHRR). Met Mag 115:285–290

Underwood SJ, Ellord GP, Kuhnert AL (2004) A multiple-case analysis of nocturnal radiation-fog development in the central valley of California Utilizing the GOES Nighttime Fog Product. J Appl Meteorol 43:297–311

Wærsted EG, Haeffelin M, Dupont J-C, Delanoë J, Dubuisson P (2017) Radiation in fog: quantification of the impact on fog liquid water based on ground-based remote sensing, Atmos. Chem Phys 17:10811–10835

Yan S, Zhu B, Kang H (2019) Long-term fog variation and its impact factors over polluted regions of East China. J. G. R.: Atmos 124:1741–1754

Zhang C, Wang Y, Hamilton K (2011) Improved representation of boundary layer clouds over the southeast pacific in ARW-WRF using a modified Tiedtke cumulus parameterization scheme. Mon Weather Rev 139:3489–3513

Zhou B, Du J (2010) Fog prediction from a multimodel mesoscale ensemble prediction system. Weather Forecast 25:303–322

Zhou Z, Deng Y, Hu Y, and Kang Z (2020) Simulating heavy meiyu rainfall: a note on the choice of the model microphysics scheme. Adv Meteorol. https://doi.org/10.1155/2020/8827071